HTLV-1 Tax induces PINK1-Parkin-dependent mitophagy to mitigate activation of the cGAS-STING pathway

Suchitra Mohanty[1,*,#], Sujit Suklabaidya[1,*], Nelli Mnatsakanyan[1], Steven Jacobson[2] and Edward W. Harhaj[1,#]

[1]Department of Cell and Biological Systems, Penn State College School of Medicine, Hershey, PA 17033, USA

[2]Viral Immunology Section, National Institute of Neurological Disorders and Stroke, National Institutes of Health, Bethesda, MD 20892, USA

*Equal contribution

Running Title: HTLV-1 Tax induces mitophagy

Keywords: HTLV-1, Tax, mitophagy, mitochondria, Parkin, NEMO, NDP52, cGAS, STING

[#]To whom correspondence should be addressed: ewh110@psu.edu or dr.suchitra26@gmail.com

Abstract

Human T-cell leukemia virus type 1 (HTLV-1) is the causative agent of adult T-cell leukemia/lymphoma (ATLL) and the neuroinflammatory disease, HTLV-1-associated myelopathy/tropical spastic paraparesis (HAM/TSP). The HTLV-1 Tax regulatory protein plays a critical role in HTLV-1 persistence and pathogenesis; however, the underlying mechanisms are poorly understood. Here we show that Tax dynamically regulates mitochondrial reactive oxygen species (ROS) and membrane potential to trigger mitochondrial dysfunction. Tax is recruited to damaged mitochondria through its interaction with the IKK regulatory subunit NEMO and directly engages the ubiquitin-dependent PINK1-Parkin pathway to induce mitophagy. Tax also recruits autophagy receptors NDP52 and p62/SQSTM1 to damaged mitochondria to induce mitophagy. Furthermore, Tax requires Parkin to limit the extent of cGAS-STING activation and suppress type I interferon (IFN). HTLV-1-transformed T cell lines and PBMCs from HAM/TSP patients exhibit hallmarks of chronic mitophagy which may contribute to immune evasion and pathogenesis. Collectively, our findings suggest that Tax manipulation of the PINK1-Parkin mitophagy pathway represents a new HTLV-1 immune evasion strategy.

Introduction

Human T-cell leukemia virus type 1 (HTLV-1) infects 10-20 million people worldwide, predominantly in endemic regions in Japan, Africa, the Caribbean, and Central/South America. HTLV-1 infection is the causative agent of adult T-cell leukemia/lymphoma (ATLL), an aggressive neoplasm of CD4+CD25+ T cells, in about 5% of infected individuals after a prolonged latent period of ~60 years[1, 2]. HTLV-1 is also associated with inflammatory disorders, most notably HTLV-1-associated myelopathy/tropical spastic paraparesis (HAM/TSP)[3]. Currently, there is no vaccine for HTLV-1, and existing treatments for ATLL and HAM/TSP are largely ineffective, emphasizing the urgent need for targeted therapies[4]. A deeper understanding of how HTLV-1 evades immune responses and persists in the host could lead to the development of novel antiviral strategies.

The HTLV-1 genome encodes structural proteins (Gag) and enzymes (Pol), along with regulatory proteins Tax and HBZ, which are crucial for viral persistence and pathogenesis[5, 6]. Tax regulates viral gene expression by recruiting CREB/ATF transcription factors and coactivators CBP/p300 to the 5' long terminal repeat (LTR) and induces oncogenic transformation by disrupting cell cycle checkpoints, inhibiting tumor suppressors and chronically activating cell signaling pathways such as NF-κB to promote the clonal proliferation and survival of infected T cells[5]. Additionally, Tax suppresses innate immune activation by targeting RIG-I-like receptor (RLR) RNA sensing and cGAS-STING DNA sensing pathways, further contributing to viral persistence[7-9]. Tax expression is tightly regulated and often silenced to evade immune detection, but stressors such as hypoxia and oxidative stress activate p38-MAPK signaling to trigger its reactivation, thus sustaining viral persistence[10-12].

Tax directly interacts with the IκB kinase (IKK) regulatory subunit IKKγ/NEMO to persistently activate NF-κB signaling that enhances cell survival and proliferation[13]. Tax-induced NF-κB activation is also linked to dysregulated autophagy and the accumulation of LC3+ autophagosomes to increase HTLV-1 production[14-17]. Tax recruits key autophagy regulators, including Beclin (BECN1) and Bif-1, to lipid raft domains through its interaction with PI3KC3, facilitating autophagosome formation[17]. Notably, BECN1 is critical for sustaining NF-κB and STAT3 activity[18], highlighting the intricate relationship between HTLV-1 infection, autophagy, and oncogenesis. Furthermore, Tax induces reactive oxygen species (ROS) production, leading to oxidative stress and DNA damage[19, 20]. Although Tax has been shown to interact with multiple mitochondrial proteins[21, 22], the precise source of Tax-induced ROS and the mechanisms by which HTLV-1 mitigates chronic oxidative stress are unknown. A more refined understanding of how Tax influences mitochondrial dynamics and dysregulated autophagy is critical to understand the mechanisms underlying HTLV-1 persistence and to develop more efficacious targeted therapies for HTLV-1-associated diseases.

Mitochondria are dynamic organelles critical for energy production and metabolism and also function as key signaling hubs for innate immune responses[23]. Mitochondrial quality control is maintained by fission and fusion and the removal of damaged mitochondria by autophagy (mitophagy)[24]. Certain viruses promote the accumulation of dysfunctional mitochondria during viral replication due to excessive ROS production and disrupted mitochondrial dynamics[25, 26]. These damaged mitochondria are not only compromised in energy production but can also trigger ROS-mediated oxidative damage and inflammation through the release of mitochondrial DNA (mtDNA)[27]. Therefore, certain viruses exploit mitophagy to dampen inflammation and immune activation to promote persistent viral infection. Mitophagy is a critical process that ensures the

timely and selective removal of damaged mitochondria through the coordination of specific mitophagy receptors and autophagy machinery. The most well-characterized mitophagy pathway is the ubiquitin (Ub)-dependent PINK1-Parkin pathway[28]. In the absence of mitochondrial stress, PTEN-induced kinase 1 (PINK1) is imported into healthy mitochondria and is rapidly degraded. However, when mitochondria undergo a loss of mitochondrial membrane potential (MMP) due to damage, PINK1 accumulates on the outer mitochondrial membrane (OMM)[29, 30]. This accumulation triggers the phosphorylation and activation of Parkin, an E3 ubiquitin ligase, which is recruited to damaged mitochondria[31]. Parkin then ubiquitinates OMM proteins, including mitofusins 1 and 2 (MFN1/2), mitochondrial Rho-GTPase 1 (Miro1), and voltage-dependent anion channel 1 (VDAC1)[32-34]. These ubiquitinated proteins are then phosphorylated by PINK1, which amplifies the signal and recruits more Parkin, thereby increasing the number of ubiquitin chains on the damaged mitochondria[35, 36]. The ubiquitinated mitochondria are recognized by autophagy receptors NDP52, OPTN, and p62/SQSTM1 through their ubiquitin binding domains and orchestrate the engulfment of damaged mitochondria in mitophagosomes that fuse with lysosomes to degrade the contents[37]. Many viruses, including Epstein-Barr virus (EBV), influenza A, HIV-1, hepatitis B virus (HBV) and hepatitis C virus (HCV) manipulate mitophagy to maintain survival of virus-infected cells and evade immune detection by suppressing inflammation and limiting oxidative stress[38-42]. However, whether HTLV-1 modulates mitochondrial dynamics as an immune evasion strategy has not yet been investigated.

In this study, we show that HTLV-1 Tax induces mitophagy to remove ROS-damaged mitochondria and mitigate innate immune activation. Tax is directly recruited to mitochondria by NEMO binding and directly engages the PINK1-Parkin pathway to initiate mitophagy. Furthermore, we identify

NDP52 as a novel interacting partner of Tax that facilitates the recruitment of damaged mitochondria to autophagosomes for degradation.

Results

Tax dynamically regulates ROS and mtROS levels and disrupts mitochondrial membrane potential

Previous studies have shown that Tax upregulates cellular ROS levels[19, 20]; however, the source of the ROS and potential impact on mitochondria in T cells have not been examined. To address these gaps in knowledge, we used Jurkat Tax Tet-On cells[21] to inducibly express Tax after doxycycline (DOX) treatment. Tax expression was confirmed after treatment with Dox for 48 h (Fig. 1A). There was no significant cytotoxicity with DOX treatment in either Jurkat Tax Tet-On or Jurkat wild-type (WT) cells (Supplementary Fig. 1A and B). We next stained cells with CellROX which exhibits bright fluorescence when oxidized by ROS, and then subjected cells to flow cytometry. As expected, ROS was increased at 24 and 48 h after Tax induction (Fig. 1B). Although ROS levels were elevated at 48 h compared to control untreated cells, there was a decrease in ROS levels at 48 h compared to 24 h DOX treatment (Fig. 1B and 1C). However, there was no change in ROS levels in WT Jurkat cells treated with DOX for the same time points, indicating that ROS accumulation is due to Tax expression in Jurkat Tax Tet-On cells (Supplementary Fig. 1C). Most of the cellular ROS (~90%) is generated by mitochondria during oxidative phosphorylation. To determine if Tax-induced ROS was derived from mitochondria, cells were stained with MitoSOX, a mitochondrial superoxide indicator specifically targeted to mitochondria. Interestingly, mitochondrial ROS (mtROS) was increased within 24 h after Tax induction but was subsequently decreased after 48 h (Fig. 1D and E). Therefore, Tax initially triggers mtROS which are then downregulated by an unknown mechanism.

Elevated ROS levels can trigger the opening of the mitochondrial permeability transition pore, leading to membrane depolarization. To assess changes in mitochondrial membrane potential (ΔΨm), we stained Jurkat Tax Tet-On cells with TMRM (Tetramethylrhodamine, Methyl Ester), a cell-permeable, cationic fluorescent dye that accumulates in active mitochondria with intact membrane potential. There was a significant decrease in ΔΨm upon Tax induction at both 24 and 48 h, as indicated by decreased TMRM fluorescence (Fig. 1F and G). In contrast, no significant change in ΔΨm was detected in WT Jurkat cells following DOX treatment for the same time points, indicating that mitochondrial depolarization is specifically induced by Tax expression (Supplementary Fig. 1D). Thus, Tax disrupts mitochondrial membrane potential and dynamically regulates ROS production, possibly by promoting the clearance of dysfunctional mitochondria.

Tax induces complete mitophagy to clear damaged mitochondria

To investigate a potential role of Tax in mitochondrial clearance we used a tandem GFP-RFP-Mito reporter where a mitochondrial targeting signal sequence is fused in frame with eGFP and RFP genes[41]. This reporter can be used to identify mitophagolysosomes based on differences in pH. GFP fluorescence (but not RFP) is quenched in the low pH of acidic mitophagolysosomes, therefore cells with complete mitophagy will only emit RFP (Red) fluorescence (no GFP), whereas cells not undergoing complete mitophagy will exhibit both GFP and RFP fluorescence observed as yellow in the merged channels. As expected, cells transfected with an empty vector and the GFP-RFP-Mito reporter exhibited yellow fluorescence in the GFP/RFP merged channels (Fig. 2A). As a positive control for mitophagy, cells were treated with the mitochondrial uncoupler CCCP (carbonyl cyanide m-chlorophenylhydrazone), which yielded mostly red fluorescent cells as expected. Interestingly, all cells expressing Tax emitted red fluorescence indicating complete mitophagy (Fig. 2A). To detect and quantify mitophagy in live cells we used the highly sensitive

pH-dependent fluorescence probe mt-Keima, which is targeted to the mitochondrial matrix[43]. There is a large shift in the excitation peak from 404 nm to 561 nm (pH 7 to pH 4) when mitochondria are targeted to lysosomes. Indeed, we found that expression of Tax was sufficient to induce mitophagy as determined by an mt-Keima flow cytometry assay (Fig. 2B).

We next determined if Tax could target mitochondria to lysosomes in T cells using confocal microscopy. Jurkat Tax Tet-On cells were treated with DOX and stained with antibodies to Tax, a mitochondrial marker (TOM20) and a lysosomal marker (LAMP2). Cells were also treated with leupeptin to inhibit lysosomal degradation. In the presence of Tax, mitochondria and lysosomes were significantly colocalized (Fig. 2C and E), indicating that Tax induces the lysosomal targeting of mitochondria. To determine if Tax targeted damaged mitochondria to autophagosomes, Jurkat Tax Tet-On cells were treated with DOX to induce Tax expression and bafilomycin A1 (BafA1) to inhibit lysosomal acidification and prevent the fusion of autophagosomes with lysosomes, followed by staining with antibodies specific for TOM20, Tax and LC3 to label autophagosomes. There was a significant colocalization of mitochondria with LC3 in Tax-expressing cells as confirmed by an overlap in intensity profiles and Manders' coefficient analysis (Fig. 2D and F). Furthermore, there was a marked increase in LC3 puncta-positive mitochondria, indicating mitophagosome formation, when Tax was expressed providing further evidence of mitophagy initiation (Fig. 2G). We also examined the expression of mitochondrial proteins by western blotting to examine Tax-induced degradation of mitochondria in Jurkat Tax Tet-On cells. Tax expression did not have a significant effect on levels of mitochondrial proteins at 24 h after induction but decreased the expression of mitochondrial proteins MTCO2 and TOM20 48 h after induction (Fig. 2H). The effect of Tax on mitochondrial proteins was specific since treatment of Jurkat cells with DOX had no effect on the levels of mitochondrial proteins (Supplementary Fig. 1E).

Ultrastructural analysis of mitochondrial dynamics in Tax-expressing T cells

To examine the effect of Tax on mitochondrial dynamics and ultrastructure, we performed transmission electron microscopy (TEM). In untreated Jurkat Tax Tet-On cells, mitochondria exhibited a normal morphology with a tubular shape and well-defined cristae (Fig. 3A). In contrast, in DOX-treated Jurkat Tax Tet-On cells there were many damaged/dysfunctional mitochondria, with autophagosomes engulfing mitochondria and forming mitophagosomes indicative of mitophagy induction (Fig. 3B). A similar phenotype characterized by irregular cristae and abundant mitophagosomes was observed in CCCP-treated Jurkat Tax Tet-On cells (Fig. 3C). Additionally, Tax-expressing cells exhibited profound cristae disorganization and membrane fragmentation, with pore formation eliciting mitochondrial content leakage into the cytoplasm (Fig. 3D–F). Early autophagophores were detected near damaged mitochondria, along with numerous mitophagosomes and mitophagolysosomes/heterolysosomes (Fig. 3G–I). TEM analysis further revealed that damaged mitochondria exhibited swelling, loss of electron-dense matrix content, and a significant increase in electron-translucency accompanied with an increase in mitophagosomes in Tax expressing cells, indicative of mitophagy (Fig. 3J-L). However, we did not observe a difference in the total number of mitochondria per cell, raising the possibility that Tax could potentially induce mitochondrial biogenesis to maintain mitochondrial function and prevent excessive mitochondrial loss (Supplementary Fig. 2A).

Certain viruses induce fission to isolate and clear damaged mitochondria by mitophagy, thus preserving mitochondrial mass and energy production while evading immune responses[44]. DRP1 (Dynamin-related protein 1) plays a key role in mitochondrial fission, a process often hijacked by viruses to enhance viral replication[41, 42]. DRP1 phosphorylation promotes its activation and mitochondrial fission[45]; however, the expression and phosphorylation of DRP1 (pDRP1) in the

context of HTLV-1 infection is unknown. Surprisingly, there was decreased pDRP1 with no change in total DRP1 expression in DOX-treated Jurkat Tax Tet-On cells (Supplementary Fig. 2B). However, blocking autophagy with BafA1 treatment did not rescue the loss of pDRP1 (Supplementary Fig. 2C). Furthermore, DRP1 was not detected in a purified mitochondrial fraction from DOX-induced Jurkat Tax Tet-On cells as shown by western blotting (Supplementary Fig. 2D), supporting the notion that Tax-induced mitophagy occurs independently of DRP1-mediated fission.

Tax-induced mitophagy is independent of ROS

We next sought to determine if Tax-induced mitophagy was dependent on ROS induction which could be indicative of an indirect mechanism of mitophagy induction. To investigate the role of ROS in Tax-induced mitophagy we treated DOX-induced Jurkat Tax Tet-On cells with N-acetylcysteine (NAC), a potent antioxidant and ROS scavenger, and confirmed a reduction in ROS levels at 24 and 48 h (Fig. 4A). However, NAC did not rescue mitochondrial depolarization in Tax-expressing cells, suggesting that Tax-mediated mitochondrial depolarization is independent of ROS accumulation (Fig. 4B and C). NAC treatment also did not prevent Tax-induced degradation of mitochondrial proteins MTCO2 and HSP60, providing additional evidence that Tax-mediated mitophagy can occur independently of ROS (Fig. 4D). Furthermore, expression of Tax in 293T cells did not increase ROS levels as shown by CellROX Deep Red staining, suggesting that ROS induction by Tax is cell-type specific (Fig. 4E and F). Nevertheless, Tax expression potently induced mitophagy in 293T cells (Fig. 2A and B), indicating that Tax-mediated mitophagy occurs independently of ROS in these cells. Additionally, we transfected an HTLV-1 proviral clone (ACH.WT)[46] into 293T cells and examined the expression of mitochondrial proteins by western blotting. The HTLV-1 proviral clone triggered MTCO2, TOM20 and HSP60 degradation and was

associated with Tax expression (Fig. 4G), further supporting the notion that Tax-induced mitophagy is independent of ROS. Collectively, these results strongly suggest that ROS is dispensable for Tax-induced mitophagy and point to a direct mechanism of mitophagy induction by Tax.

Tax triggers Parkin-mediated mitophagy

Since the PINK1/Parkin pathway is critical for mitochondrial quality control through mitophagy, we next examined potential roles of PINK1 and Parkin in Tax-induced mitophagy. Inducible expression of Tax in Jurkat Tax Tet-On cells correlated with a decrease in PINK1 and Parkin expression 48 h after induction, suggesting that Tax may promote the degradation of both PINK1 and Parkin in mitophagosomes (Fig. 5A). Indeed, Tax expression caused Parkin translocation to mitochondria as shown by western blotting of mitochondrial fractions (Fig. 5B). We next performed confocal microscopy using Jurkat Tax Tet-On cells that were untreated or treated with DOX and stained with antibodies to Tax, TOM20 and Parkin. In the presence of Tax, there was enhanced Parkin colocalization with mitochondria as revealed by significant overlap in intensity profile plots and Manders' coefficient analysis (Fig. 5C-E and Supplementary Fig. 3A).

To determine the functional significance of Parkin in Tax-induced mitophagy, we generated stable Parkin knockdown (sh-Parkin-Jurkat Tax Tet-On) or scrambled shRNA control (sh-Control) cells using lentiviral-mediated shRNA delivery (Supplementary Fig. 3B and 3C). Upon Tax expression by DOX treatment, Parkin knockdown cells exhibited minimal mitochondrial protein degradation, indicating that Parkin deficiency blocked Tax-induced mitophagy (Fig. 5F). We next used HeLa cells, which lack endogenous Parkin expression, to study Parkin-dependent mitophagy upon its exogenous expression. Confocal microscopy analysis revealed robust Tax-mediated recruitment of Parkin to mitochondria (Fig. 5G). Furthermore, co-expression of Tax and Parkin triggered

mitochondrial protein degradation in HeLa cells that was not apparent with the expression of either Tax or Parkin alone (Fig. 5H). To further substantiate the role of Parkin in mitophagy, we examined mitophagosome formation in response to Tax expression by performing confocal microscopy using HeLa cells stably expressing LC3-GFP. Notably, the combined expression of Tax and Parkin led to the recruitment of mitochondria to LC3-positive autophagosomes, forming mitophagosomes and facilitating the autophagic degradation of mitochondria (Fig. 5I). In contrast, expression of Tax or Parkin alone did not significantly promote mitophagosome formation, supporting the hypothesis that Tax induces Parkin-dependent mitophagy (Fig. 5I).

Tax promotes constitutive Parkin-dependent mitophagy in HTLV-1 transformed T cells and PBMCs from HAM/TSP patients

To investigate Tax-induced mitophagy in HTLV-1-transformed T cells, we performed confocal microscopy using C8166 cells and stained for endogenous LC3, Tax and the mitochondrial marker TOM20 in the absence of BafA1 or leupeptin. Jurkat cells served as a negative control and were processed with an identical staining protocol. In C8166 cells, there was a strong colocalization of LC3 puncta with mitochondria, forming mitophagosomes indicative of constitutive mitophagy (Fig. 6A). In contrast, Jurkat cells exhibited diffuse LC3 staining with no detectable colocalization with mitochondria, confirming the absence of mitophagic activity as supported by intensity profile plots and Manders' coefficient analysis (Fig. 6A–C). To further evaluate Parkin recruitment to mitochondria, we stained C8166 and Jurkat cells for Parkin, Tax and TOM20. Confocal microscopy revealed significant mitochondrial localization of Parkin in C8166 cells as revealed by overlap in the intensity profiles and Manders' coefficient analysis (Fig. 6D–F). Conversely, Jurkat cells did not exhibit detectable Parkin colocalization with mitochondria (Fig. 6D-F), suggesting the selective activation of constitutive mitophagy in HTLV-1-transformed cells. We

then extended these findings to primary cells from HTLV-1-infected individuals using peripheral blood mononuclear cells (PBMCs) from HAM/TSP patients and uninfected controls. Indeed, there was a marked reduction in mitochondrial proteins and Parkin expression in HAM/TSP PBMCs compared to controls, indicative of mitophagy (Fig. 6G, low exposure). Interestingly, HAM/TSP PBMCs exhibited elevated levels of a modified (likely ubiquitinated) form of Parkin (Fig. 6G, high exposure). In the early stages of mitophagy, PINK1 phosphorylates Ub on Ser65 to activate Parkin E3 ligase activity[47, 48]. Phospho-ubiquitin levels were significantly increased in HAM/TSP PBMCs (Fig. 6H) compared to control PBMCs, further indicating chronic mitophagic activity in HAM/TSP PBMCs.

Tax localizes to mitochondria and interacts with PINK1 and Parkin to initiate mitophagy

Given that Tax can induce mitophagy in the absence of ROS, we next investigated its potential mitochondrial localization by performing confocal microscopy using untreated and DOX-treated Jurkat Tax Tet-On cells stained with antibodies specific for TOM20 and Tax. In DOX-treated cells, there was a pronounced colocalization of Tax with mitochondria, as confirmed by overlap in intensity profiles and Manders' coefficient analysis (Fig. 7A-C). In line with these results, our previous study demonstrated mitochondrial localization of Tax in HTLV-1-transformed MT-2 cells and in 293T cells transiently transfected with Tax[21]. To further investigate Tax mitochondrial localization, we isolated mitochondrial fractions from untreated and DOX-treated Jurkat Tax Tet-On cells and performed western blotting for Tax expression. A substantial amount of Tax was detected in the mitochondrial fraction of DOX-treated cells, thus confirming its mitochondrial localization (Fig. 7D). We next asked if the mitochondrial localization of Tax was dependent on Parkin translocation to mitochondria. To address this question, HeLa cells were transiently transfected with Tax and/or Parkin, and mitochondrial fractions were isolated for western blotting.

Tax localized to mitochondria regardless of Parkin expression, indicating that the mitochondrial localization of Tax is independent of Parkin recruitment to mitochondria (Fig. 7E).

To understand the mechanisms by which Tax regulates the PINK1-Parkin pathway, we performed co-immunoprecipitation (co-IP) assays to determine if Tax interacted with PINK1 and/or Parkin in HTLV-1 transformed C8166 cells. Tax was detected in anti-PINK1 and anti-Parkin immunoprecipitates, and reciprocal co-IPs further validated these interactions (Fig. 7F and G). Interestingly, multiple modified forms of Parkin (likely ubiquitinated) were detected in Tax immunoprecipitates (Fig. 7G) suggesting that Tax may preferentially interact with ubiquitinated Parkin to facilitate mitophagy. Similarly, in DOX-treated Jurkat Tax Tet-On cells, Tax was detected in anti-PINK1 and anti-Parkin immunoprecipitates, further confirming its interaction with both proteins (Fig. 7H). Finally, we took a loss-of-function approach to deplete the Tax protein in HTLV-1 transformed MT-2 cells by treating with a KDR inhibitor (SU 1498) that we recently demonstrated can promote Tax degradation[49]. Upon treatment with SU 1498, Tax expression was decreased and the mitochondrial marker MTCO2 was correspondingly increased thus providing further evidence that Tax induces chronic mitophagy in HTLV-1 transformed cells (Fig. 7I). Together, these findings indicate that Tax directly engages the PINK1-Parkin pathway to induce mitophagy.

Tax is recruited to damaged mitochondria through NEMO binding

A recent study has demonstrated that NEMO is recruited to damaged mitochondria through its Ub binding domain[50]. Given that Tax strongly interacts with NEMO, we hypothesized that Tax was recruited to damaged mitochondria via NEMO. To examine the recruitment of NEMO to mitochondria, we performed immunofluorescence and confocal microscopy with antibodies specific for Tax, NEMO and the mitochondrial marker TOM20 using untreated and DOX-treated

Jurkat Tax Tet-On cells. In the presence of Tax there was a significant colocalization of NEMO with mitochondria (Fig. 8A) which was confirmed by an overlap in the intensity profiles and Manders' coefficient analysis (Fig. 8B-C and Supplementary Fig. 4A). Furthermore, there was a marked accumulation of NEMO in the mitochondrial fraction of DOX-treated Jurkat Tax Tet-On cells (Fig. 8D), providing further evidence of the recruitment of NEMO to mitochondria in cells expressing Tax.

To determine if the Tax-NEMO interaction was required to induce mitophagy, we used Jurkat-Tax M22 Tet-On cells, which inducibly express the Tax M22 point mutant (T130A, L131S) impaired in NEMO binding, NF-κB activation, ROS induction and LC3+ autophagosome accumulation[15, 20, 51]. The Tax M22 mutant had no effect on mitochondrial membrane potential (Supplementary Fig. 4B) and mitochondrial protein degradation (Fig. 8E), indicating that Tax requires NEMO binding to clear damaged mitochondria. Furthermore, mitochondrial fractionation assays revealed impaired recruitment of Tax M22 and NEMO to mitochondria (Fig. 8F). These results underscore the critical role of the Tax-NEMO interaction in the recruitment of Tax to mitochondria to trigger mitophagy. We next performed co-IP assays to determine if Tax M22 could interact with Parkin. 293T cells were transfected with plasmids expressing Tax, Tax M22 and Parkin, and lysates were immunoprecipitated using a Tax antibody. Parkin was detected in Tax, but not Tax M22, immunoprecipitates (Fig. 8G) suggesting that Tax M22 is unable to bind Parkin. Collectively, these findings establish a critical role of the Tax-NEMO complex in driving mitophagy.

Tax interacts with NDP52 to recruit damaged mitochondria to autophagosomes

The PINK1-Parkin pathway relies on selective autophagy receptors (SARs), in particular NDP52 Optineurin (OPTN), and p62/SQSTM1, to bind to and target ubiquitinated mitochondria to LC3-positive autophagosomes, which subsequently fuse with lysosomes to degrade mitochondria[37]. We

next sought to identify the SAR used by Tax to induce mitophagy by examining the expression of NDP52, NBR1, OPTN, TAX1BP1 and p62 in the absence or presence of Tax in T cells. NDP52 expression was significantly decreased in the presence of Tax whereas TAX1BP1 was only modestly decreased; NBR1 and OPTN expression increased in the presence of Tax, and p62 was unchanged (Fig. 9A). NDP52 expression was rescued together with TOM20 and LC3 by BafA1 treatment, indicating that NDP52 is likely degraded together with mitochondrial proteins (Supplementary Fig. 5A). Given that Tax interacts with multiple SARs such as p62[52] and TAX1BP1[53], we hypothesized that Tax may also interact with NDP52. We performed a co-IP assay to examine a potential interaction between Tax and NDP52 in C8166 cells. Indeed, Tax was detected in anti-NDP52 immunoprecipitates, and a reciprocal co-IP further validated these interactions (Fig. 9B). Similarly, in DOX-treated Jurkat Tax Tet-On cells, Tax was detected in anti-NDP52 immunoprecipitates (Fig. 9C), further confirming Tax interaction with NDP52. Since NDP52 is recruited to damaged mitochondria, we next examined the translocation of NDP52 to mitochondria upon Tax expression. Western blotting analysis of pure mitochondrial fractions revealed a significant amount of NDP52 associated with mitochondria in DOX-treated Jurkat Tax Tet-On cells (Fig. 9D). A previous study reported that Tax interacts with p62 for NF-κB activation to facilitate the survival and spread of HTLV-1-infected cells[52]. Interestingly, there was substantial p62 accumulation in the mitochondrial fraction of DOX-treated Jurkat Tax Tet-On cells, indicating a potential involvement of p62 in Tax-induced mitophagy along with NDP52 (Fig. 9D). To examine the recruitment of NDP52 to mitochondria, immunofluorescence and confocal microscopy was performed using untreated and DOX-treated Jurkat Tax Tet-On cells. As expected, there was significant colocalization of NDP52 with the mitochondria (TOM20) in the presence of Tax (Fig. 9E), and this was confirmed by the overlap in intensity profiles and Manders' coefficient

355 analysis (Fig. 9F and G). Next, we used HeLa pentaKO cells that are deficient for NDP52, p62,
356 NBR1, TAX1BP1 and OPTN, and are ideal for studying the functional significance of specific
357 SARs by add-back experiments without potential interference from endogenous SARs [37]. We
358 confirmed knockout of all five SARs by western blotting (Supplementary Fig. 5B). HeLa pentaKO
359 cells were transfected with Tax and Parkin plasmids in combination with NDP52, TAX1BP1 or
360 p62 and then examined the expression of MTCO2 by western blotting to determine the functional
361 significance of these SARs in Tax-mediated mitophagy. Both NDP52 and p62 promoted the
362 degradation of MTCO2 in the presence of Tax and Parkin in HeLa pentaKO cells (Fig. 9H),
363 suggesting that NDP52 and p62 are the critical SARs for Tax-induced mitophagy. Collectively,
364 these results indicate that Tax interacts with SARs, in particular NDP52 and p62, to clear damaged
365 mitochondria by mitophagy.

366 **Tax induces mitophagy to mitigate cGAS-STING activation**

367 Damaged mitochondria release mtDNA into the cytosol that can activate the cGAS-STING DNA
368 sensing pathway and the NLRP3 inflammasome[54, 55]. To examine the effect of Tax on cytoplasmic
369 mtDNA leakage, we selectively permeabilized the plasma membrane using an optimized
370 concentration of NP-40, ensuring the integrity of both the mitochondrial and nuclear membranes.
371 This approach allowed for the isolation of a pure cytoplasmic fraction, free of mitochondrial and
372 nuclear DNA contamination. Indeed, western blotting analysis confirmed the absence of
373 mitochondrial (TOM20, MTCO2) and nuclear (Lamin B2) markers in the cytoplasmic fraction,
374 while β-Actin was detected in both the cytoplasmic and residual fractions, validating the purity of
375 the isolation method (Fig. 10A). To investigate the effect of Tax expression and Parkin-dependent
376 mitophagy on mtDNA release, we performed quantitative real-time PCR (qRT-PCR) of the D-loop
377 region of mtDNA using the purified cytoplasmic fraction from untreated and DOX-treated sh-

Control and sh-Parkin Jurkat Tax Tet-On cells. There was a significant reduction in cytoplasmic mtDNA induced by Tax expression (Fig. 10B); however, the Tax-mediated decrease in cytoplasmic mtDNA was impaired in Parkin-knockdown cells (Fig. 10B).

It is well established that Tax blocks the induction of IFN-β to suppress innate immune activation[7]. Indeed, DOX-induced expression of Tax in sh-Control Jurkat Tax Tet-On cells dampened basal *Ifnb* mRNA levels; however, Tax-mediated inhibition of *Ifnb* was partially impaired when Parkin was knocked down (Fig. 10C). These data indicate that Tax utilizes mitophagy as a mechanism to limit mtDNA release into the cytoplasm and dampen IFN-β production. To extend these findings, we treated sh-Control and sh-Parkin Jurkat Tax Tet-On cells (+/- DOX) with the STING agonist diABZI (2,3-diaminobenzothiazol) compound 3 to activate the STING pathway and quantified *Ifnb* mRNA expression by qRT-PCR. Although Tax downregulated basal *Ifnb* expression as expected, diABZI-induced *Ifnb* expression was potentiated in the presence of Tax (Fig. 10D). This was unexpected and likely due to Tax-mediated genotoxic and mitochondrial stress priming cGAS-STING signaling. Nevertheless, when Parkin was knocked down, diABZI-induced *Ifnb* expression at 2h in the presence of Tax was significantly enhanced (Fig. 10D) suggesting that Tax utilizes Parkin and mitophagy to limit the extent of STING-mediated type I IFN induction. The observed effects were specific to Tax since DOX treatment of Jurkat cells did not enhance diABZI-induced *Ifnb* expression (Supplementary Fig. 6). To investigate the impact of Tax-induced mitophagy on cGAS-STING signaling, western blotting was performed using phospho-STING and phospho-IRF3 antibodies with lysates from diABZI-stimulated sh-Control and sh-Parkin Jurkat Tax Tet-On cells (+/- DOX). Consistent with the *Ifnb* qRT-PCR experiment (Fig. 10D), there was a marked increase in diABZI-induced STING and IRF3 activation in the presence of Tax and control shRNA and this was further enhanced in Parkin knockdown cells (Fig. 10E). STING activation in T cells

triggers cell death[56, 57]. Consistent with prior studies, diABZI-induced apoptosis in T cells was detected by cleaved PARP1 (Fig. 10E); however, Tax suppressed STING-mediated cell death, but this was independent of Parkin (Fig. 10E). Together, these findings suggest that Parkin-dependent mitophagy restrains Tax-mediated activation of the cGAS-STING pathway but Tax inhibits STING-induced cell death by other mechanisms.

Discussion

Our study has revealed a novel role of HTLV-1 Tax in the clearance of damaged mitochondria through Parkin-dependent mitophagy. Our data support a model (Fig. 10F) whereby Tax is recruited to damaged mitochondria through NEMO binding, and Tax then facilitates the translocation of Parkin to damaged mitochondria, potentially through its interactions with PINK1 and Parkin. Tax then interacts with autophagy receptors such as NDP52 to recruit LC3+ autophagosomes to damaged mitochondria marked with polyubiquitin chains. Tax-induced mitophagy likely serves as an immune evasion strategy to dampen type I IFN responses mediated by cGAS-STING signaling.

Transformed cells maintain a delicate balance of ROS production to drive signal transduction pathways and metabolism while enhancing antioxidant defenses to prevent ROS-induced cell death[58]. Tax upregulation of ROS elicits genomic instability through DNA damage and apoptosis is blocked in part by Tax interacting with the deubiquitinase USP10[19, 20]. We previously identified several potential Tax-binding mitochondrial proteins through LC/MS analysis and found that Tax hijacks TRAF6 to stabilize MCL-1 via K63-linked polyubiquitination in mitochondria [21, 22]. Here we found that Tax dynamically regulates mitochondrial ROS production and mitochondrial membrane potential in a temporal manner. Given the detrimental effects of persistent elevated ROS levels, it is likely that Tax has evolved a mechanism to clear ROS-damaged, depolarized

mitochondria by mitophagy to promote viral persistence. A previous study has shown that Tax directly promotes IKK-dependent assembly of LC3+ autophagosomes by interacting with the autophagy regulatory complex, including BECN1 and Bif-1[17]. Additionally, Tax enhances autophagosome accumulation by preventing their fusion with lysosomes, thereby inhibiting the degradation of autophagic components and promoting HTLV-1 replication[14]. Congruent with previous studies that Tax manipulates autophagy to support the survival and transformation of HTLV-1-infected T cells, Tax similarly promotes the autophagic degradation of damaged mitochondria that is likely beneficial for viral persistence.

A growing body of evidence suggests that multiple viruses manipulate mitophagy to facilitate their replication and evade host immune responses[59]. Both HBV and HCV disrupt mitochondrial dynamics by promoting the phosphorylation of DRP1 at Ser616, a modification that enhances mitochondrial fission and triggers ubiquitin-dependent mitophagy[41, 42]. Regarding HBV, the HBx protein interacts with and upregulates Parkin expression[60], while the non-structural protein 5A of HCV promotes the mitochondrial translocation of Parkin to initiate mitophagy[61]. Similarly, the EBV-encoded BHRF1 protein stimulates mitophagy through DRP1-mediated mitochondrial fission and inhibits IFN-β induction by recruiting Parkin to mitochondria[38]. Varicella zoster virus (VZV) glycoprotein E serves as an antagonist of IFN-β induction by promoting PINK1-Parkin-dependent mitophagy, effectively blocking MAVS and STING-mediated innate immune signaling[62]. Taken together, our study adds to a growing body of knowledge of viral subversion of mitophagy as a mechanism to enhance viral persistence. We demonstrated that HTLV-1 Tax directly engages the PINK1-Parkin pathway to promote Parkin mitochondrial translocation to initiate mitophagy (Fig. 7). Although we did not identify a clear link between DRP1 phosphorylation and mitophagy in HTLV-1-infected cells (Supplementary Fig. 2), its role in

mitochondrial dynamics warrants further investigation, given its involvement in viral modulation of mitochondria. Intriguingly, our data indicate that Tax-induced mitophagy can occur independently of ROS accumulation, as NAC-treated cells still exhibited mitochondrial protein degradation upon Tax expression (Fig. 4), contrasting with the ROS-dependent mitophagy observed in many other viral infections[61-64]. Furthermore, we detected hallmarks of constitutive mitophagy in HTLV-1 transformed T cell lines and PBMCs from HAM/TSP patients (Fig. 6) suggesting a pivotal role of mitophagy in maintaining persistent infection and potentially disease-associated pathology. Moreover, Tax expression increases in response to stress stimuli, such as hypoxia[65]; therefore, HTLV-1-infected T cells that traffic to poorly oxygenated tissues such as lymph nodes and bone marrow likely encounter a favorable environment for viral replication and *de novo* infections. A previous study demonstrated that cancer cells adapt to the hypoxic microenvironment by inducing mitophagy through PINK1 stabilization and Parkin translocation, supporting the metabolic shift toward glycolysis[66]. Therefore, it is plausible that Tax induces mitophagy in hypoxic conditions to maintain cellular energy homeostasis for the survival of HTLV-1-infected T cells when exposed to stress.

Tax binds to NEMO in the IKK complex to trigger chronic NF-κB activation, inflammation and viral-mediated T cell transformation[13, 67, 68]. Interestingly, the Tax M22 mutant deficient in NEMO binding and NF-κB activation[51] is also impaired in the induction of ROS[20] and LC3+ autophagosomes[15], thus linking the Tax-NEMO complex and NF-κB activation to autophagy dysregulation in HTLV-1-infected T cells. A recent study showed that NEMO is recruited to depolarized mitochondria in a Parkin-dependent manner after oxidative damage to trigger inflammatory signaling through the IKK complex and upregulation of NF-κB target genes[50]. We found substantial recruitment of NEMO to mitochondria following Tax expression, and our

findings indicate that Tax-NEMO binding is essential for mitophagy induction as the Tax M22 mutant failed to induce mitochondrial depolarization and interact with Parkin (Fig. 8). These results indicate that the Tax-NEMO interaction serves a critical step in triggering Parkin-dependent mitophagy in the context of HTLV-1 infection and further suggest that NEMO recruits Tax to damaged mitochondria by sensing polyubiquitin chains that are conjugated to these mitochondria. An intriguing possibility is that mitophagy triggered by the Tax-NEMO complex may contribute to the activation of chronic IKK/NF-κB activation and inflammation, with potential relevance for HAM/TSP disease pathogenesis.

NDP52 plays a critical role in Parkin-dependent mitophagy by recognizing ubiquitin-tagged damaged mitochondria and recruiting autophagic machinery (i.e., LC3 and p62), thereby promoting autophagosome formation and fusion with lysosomes for the degradation of dysfunctional mitochondria[37, 69]. A previous study has shown that Tax interacts with p62 to promote activation of NF-κB[52], but its role in Tax-induced autophagy dysregulation remains poorly understood. Here we identified NDP52 as a key binding partner of Tax and demonstrated its key function in the recruitment of damaged mitochondria for autophagic clearance. Notably, we observed a coordinated mitochondrial localization of both p62 and NDP52, and experiments in HeLa pentaKO cells suggest that these two SARs collaborate in Tax-mediated mitophagy (Fig. 9D, H). Our findings highlight the complexity of autophagy regulation by HTLV-1 and provide new insight into the mechanisms by which Tax manipulates multiple autophagy receptors to facilitate the selective degradation of dysfunctional mitochondria.

Upon mitochondrial damage, the diminished mitochondrial membrane potential triggers the release of DAMPs such as mtDNA and cytochrome c. The leaked cytosolic mtDNA is sensed by cGAS which then activates STING, TBK1 and IRF3 to upregulate the expression of type I IFN [55,

493 [70]. Additionally, cytosolic mtDNA can contribute to the activation of the NLRP3 inflammasome,
494 leading to the secretion of caspase-1-dependent pro-inflammatory cytokines IL-1β and IL-18[71].
495 However, it is unclear if Tax has any role in regulating the NLRP3 inflammasome. Parkin-mediated
496 mitophagy plays a critical role in preventing cytosolic mtDNA which could trigger aberrant innate
497 immune signaling activation and inflammation [72, 73]. In support of these findings, we observed
498 decreased levels of cytosolic mtDNA following Tax expression, and Parkin knockdown increased
499 mtDNA accumulation and type I IFN induction, suggesting a critical role of mitophagy in limiting
500 mtDNA release into the cytosol to mitigate aberrant innate immune activation. Furthermore, Parkin
501 deficiency also enhanced STING and IRF3 activation following Tax expression, further suggesting
502 a pivotal role of mitophagy in mitigating cGAS-STING signaling and the induction of type I IFN.
503 It was surprising that Tax expression was associated with enhanced diABZI-induced STING
504 activation (Fig. 10D, E), and this can likely be attributed to Tax-mediated genotoxic and/or
505 mitochondrial stress priming the cGAS-STING pathway for activation. In this context, Parkin
506 plays a key role in limiting the extent of STING activation when Tax is expressed. Although a
507 previous study showed that Tax inhibits STING signaling, these conclusions were based on
508 overexpression experiments in 293T cells[8]. Nevertheless, we did find that Tax potently suppresses
509 STING-induced T cell death (Fig. 10E), but this is independent of Parkin and may be due to Tax
510 upregulation of anti-apoptotic genes or interaction with anti-apoptotic proteins[12, 21, 74, 75]. Since Tax
511 expression can be silenced by epigenetic mechanisms to promote immune evasion and viral
512 persistence, it is conceivable that other HTLV-1-encoded proteins may also promote mitophagy
513 such as p13 which can localize to the inner mitochondrial membrane[76] or p30^{II} which has been
514 shown to mitigate oxidative damage caused by Tax and HBZ[77].

In summary, we found that Tax hijacks the PINK1-Parkin pathway to promote the clearance of damaged mitochondria and mitigate cGAS-STING activation and type I IFN induction. Furthermore, we identified a critical role of the Tax-NEMO complex in initiating ubiquitin-dependent mitophagy and uncovered NDP52 as a new interacting partner of Tax that facilitates the recruitment of ubiquitinated mitochondria to LC3+ autophagosomes for complete mitochondrial degradation. These findings provide new insight into the mechanisms by which HTLV-1 manipulates host cellular processes to evade immune surveillance and offers potential avenues for therapeutic intervention to target HTLV-1 persistence and oncogenesis.

Methods

Ethics Statement

Peripheral blood samples from HAM/TSP patients were collected under protocol #98N0047 approved by the National Institutes of Health IRB #10, IRB Registration: IRB00011862 and the National Institute of Neurological Disorders and Stroke (NINDS) Scientific Review Committee. Written informed consent was obtained from subjects prior to study inclusion in accordance with the Declaration of Helsinki.

Cell Culture, Plasmids and Antibodies

Jurkat Tax Tet-On and Jurkat Tax M22 Tet-On cells were provided by Dr. Warner Greene. C8166 cells were obtained from Dr. Shao-Cong Sun. MT-2 cells (ARP-237) were obtained from BEI Resources. Human embryonic kidney cells (HEK 293T; CRL-3216), HeLa (CCL-2) and Jurkat (T1B-152) cells were purchased from ATCC. HeLa LC3-GFP cells were provided by Dr. Wen-Xing Ding. HeLa pentaKO cells were obtained from Dr. Richard Youle. Jurkat, Jurkat Tax Tet-On, Jurkat Tax M22 Tet-On, C8166 and MT-2 cells were cultured in RPMI medium. HEK 293T, HeLa, HeLa LC3-GFP and HeLa pentaKO cells were cultured in Dulbecco's modified Eagle's medium (DMEM). The medium was supplemented with fetal bovine serum (FBS; 10%) and penicillin-streptomycin (1%). Tet System Approved FBS (Takara; 631106) was used to culture Jurkat Tax Tet-On and Jurkat Tax M22 Tet-On cells. Lenti-X 293T cells were purchased from Takara (632180) and cultured in DMEM media supplemented with 10% FBS and 1% P/S. PBMCs obtained from two patients with a clinical diagnosis of HAM/TSP were cultured in RPMI medium supplemented with FBS (10%) and penicillin-streptomycin (1%) for six days to induce Tax expression. Control PBMCs from healthy donors were cultured in RMPI medium for two days. Anti-Tax (1A3; sc-57872), NEMO (sc-8032), vinculin (sc-73614), and β-actin (sc-47778)

antibodies were purchased from Santa Cruz Biotechnology. Alexa Fluor 594-conjugated goat anti-mouse IgG (A-11005), Alexa Fluor 488-conjugated goat anti-rabbit IgG (A-11008), Alexa Fluor 647-conjugated donkey anti-rabbit IgG (A-31573), Alexa Fluor 647-conjugated donkey anti-mouse IgG (A-31571) and Alexa Fluor 405-conjugated donkey anti-mouse IgG (A48257) were purchased from Thermo Fisher Scientific. TOM20 (42406), HSP60 (12165), NDP52 (60732), NBR1 (9891), phospho-Ubiquitin (Ser65) (70973), phospho-IRF3 (4947), IRF3 (4302), phospho-STING (72971), STING (13647) and cleaved PARP (5625) were purchased from Cell Signaling Technology. MTCO2 (55070-1-AP), PINK1 (23274-1-AP), Parkin (14060-1-AP), LC3 (14600-1-AP), p62 (18420-1-AP) and TOM20-CoraLite® Plus 488 (CL488-11802) antibodies were purchased from Proteintech. TAX1BP1 antibody (ab176572) was purchased from Abcam. LAMP2 monoclonal antibody, Alexa Fluor 647 (A15464) was purchased from Thermo Fisher Scientific. ProLong Gold Antifade Mountant with DAPI (P36962), ProLong Gold Antifade Reagent (P36965) and SuperSignal West Pico PLUS Chemiluminescent Substrate (34580) were purchased from Thermo Fisher Scientific. Doxycycline (BP26535) and puromycin dihydrochloride (A1113803) were purchased from Fisher Scientific. SU 1498 (SML1193) was purchased from MilliporeSigma. diABZI compound 3 (cat# tlrl-diabzi) was purchased from InvivoGen. The pCMV4-Tax, pCMV4-Tax M22 and VSV-G plasmids were provided by Dr. Shao-Cong Sun. pHAGE-mt-mKeima was a gift from Richard Youle (Addgene plasmid # 131626; http://n2t.net/addgene:131626; RRID:Addgene_131626). CFP-Parkin was a gift from Richard Youle (Addgene plasmid #47560; http://n2t.net/addgene:47560; RRID; Addgene_47560). mCherry-Parkin was a gift from Richard Youle (Addgene plasmid #23956; http://n2t.net/addgene:23956; RRID:Addgene_23956). HA-p62 was a gift from Qing Zhong (Addgene plasmid #28027; http://n2t.net/addgene:28027; RRID:Addgene_28027). pHAGE-

eGFP-NDP52 was a gift from Wade Harper (Addgene plasmid#175749; http://n2t.net/addgene:175749; RRID:Addgene_175749). pHAGE-FLAG-APEX2-TAX1BP1 was a gift from Wade Harper (Addgene plasmid #175761; http://n2t.net/addgene:175761; RRID:Addgene_175761). psPAX2 was a gift from Didier Trono (Addgene plasmid #12260; http://n2t.net/addgene:12260; RRID:Addgene_12260). The pACH HTLV-1 proviral clone plasmid was provided by Dr. Lee Ratner. The GFP-RFP-Mito reporter plasmid was provided by Dr. Aleem Siddiqui.

Immunoblotting and co-immunoprecipitation assays

Whole-cell lysates were prepared by lysing cells in RIPA buffer (50 mM Tris-Cl [pH 7.4], 150 mM NaCl, 1% NP-40, 0.25% sodium deoxycholate, Pierce Protease and Phosphatase Inhibitor) on ice, followed by centrifugation. Cell lysates were resolved by SDS-PAGE and transferred to nitrocellulose membranes using either the Trans-Blot Turbo Transfer System (Bio-Rad) or wet transfer. Immunoblotting was performed with specific primary antibodies and HRP-conjugated mouse or rabbit secondary antibodies (Cytiva Life Sciences; NA931; NA934). Immunoreactive bands were detected with SuperSignal West Pico PLUS Chemiluminescent substrate and analyzed with a Bio-Rad ChemiDoc Imaging System. Western blot images were processed with Image Lab software (Bio-Rad Laboratories). For co-IP assays, the Dynabeads Protein G Immunoprecipitation Kit (Thermo Fisher Scientific; 10007D) was used following the manufacturer's guidelines.

Immunofluorescence and confocal microscopy

Cells were washed with PBS and seeded in poly L-lysine pre-coated coverslips (VWR, BD354085). Immunofluorescence and confocal microscopy were performed as previously described[49, 78]. Cells were fixed with 4% paraformaldehyde and permeabilized with Triton X-100. Samples were blocked with 5% BSA for 1 h followed by staining with primary antibodies

overnight at 4°C and fluorescently-conjugated secondary antibodies for 1 h at room temperature. DAPI was used to stain nuclei. Images were acquired using a Leica SP8 confocal microscope equipped with a 63x oil objective. Images were processed, analyzed and quantified using Fiji image analysis software (NCBI).

Cell viability assay

Cell viability was determined by SYTOX™ Blue Dead Cell Stain (Thermo Fisher Scientific; S34857; 1 µM), a nucleic acid stain that stains cells with compromised plasma membranes and fluoresces bright blue when excited with a 405 nm violet laser. The stain was added directly to tubes containing harvested cells, and fluorescence intensity was quantified using a BD FACSymphony A3 flow cytometer.

Mitochondrial membrane potential assay

Mitochondrial membrane potential was determined using Image-iT TMRM Reagent (Thermo Fisher Scientific; I34361, 100 nM), which accumulates in active mitochondria. Cells were incubated for 45 min at 37°C in the dark, washed three times with PBS, and stained with SYTOX™ Blue Dead Cell Stain (1 µM) to assess viability. Fluorescence intensity was quantified using a BD FACSymphony A3 flow cytometer.

Total ROS and mtROS measurement

Intracellular ROS levels were quantified using CellROX™ Deep Red (Thermo Fisher Scientific, C10422), which fluoresces upon oxidation (Ex/Em: 644/665 nm). Cells in a 6-well plate were incubated with 5 µM CellROX™ for 30 min at 37°C in the dark and then washed three times with PBS. SYTOX™ Blue Dead Cell Stain (Thermo Fisher Scientific, #S34857, 1 µM) was used to assess cell viability and ROS was quantified in live cells. Fluorescence intensity was analyzed using a BD FACSymphony A3 flow cytometer.

Mitochondrial ROS (mtROS) levels were quantified by staining with MitoSOX™ Red (Thermo Fisher Scientific; M36008), a mitochondria-targeted dye that fluoresces upon oxidation by superoxide (Ex/Em: 396/610 nm). Cells were incubated with 5 µM MitoSOX™ for 30 min at 37°C in the dark, washed three times with PBS and then incubated with 1 µM SYTOX™ Blue to assess cell viability. Fluorescence was measured using a BD FACSymphony A3 flow cytometer.

Plasmid transfections

Cells were transiently transfected with GenJet In Vitro DNA Transfection Reagent (SignaGen Laboratories) according to the manufacturer's protocol.

Isolation of mitochondrial and cytoplasmic fractions

Mitochondrial fractions were isolated from cells using the Mitochondria Isolation Kit (Thermo Fisher Scientific; #89874) according to the manufacturer's instructions. The isolated mitochondrial pellet was resuspended and lysed with 2% CHAPS in Tris-buffered saline (TBS; 25 mM Tris, 0.15 M NaCl, pH 7.2). The sample was vortexed for 2 min to ensure complete lysis, followed by centrifugation at high speed for 2 min to collect the supernatant containing the soluble mitochondrial fraction. The protein concentration in the mitochondrial fraction was determined using the BCA Protein Assay Kit (Thermo Scientific; 23225).

To isolate cytoplasmic fractions, cells were lysed with 0.02% NP40 lysis buffer (50 mM Tris-HCl, pH 7.5, 150 mM NaCl) supplemented with protease and phosphatase inhibitors. The lysate was centrifuged at 18,630 g for 20 min at 4°C to pellet cellular debris. The resulting supernatant, which contains the cytoplasmic fraction, was collected. The protein concentration in the cytoplasmic fraction was determined using the BCA Protein Assay Kit.

Lentiviral shRNA-Mediated Knockdown and Generation of Stable Cell Lines

The GIPZ Human PRKN (Parkin) shRNA plasmids (RHS4430-200235908 and RHS4430-200236334) were purchased from Horizon Discovery. Lenti-X^{TM} 293T cells were transfected with the shRNA expression vector (sh-Control or sh-Parkin), the packaging plasmid psPAX2 (gag/pol), and the envelope plasmid pMD2.G (VSV-G) at a 6:3:1 ratio. The viral supernatants were collected 72 h post-transfection and concentrated using a Lenti-X^{TM} Concentrator (Takara; 631231). Concentrated lentiviral particles were stored at -80°C until needed. Jurkat-Tax Tet-On cells were transduced with lentivirus by spinoculation and selected with puromycin (2 µg/mL). Knockdown efficiency was examined by flow cytometry and western blotting analysis.

Quantitative Real Time PCR (qRT-PCR)

Cells were harvested and processed for RNA isolation using the RNA Spin II Kit (Macherey-Nagel; 740955) according to the manufacturer's instructions. cDNA was made from RNA using M-MLV Reverse Transcriptase (Thermo Fisher Scientific; 28025-013) and Oligo (dT) (Thermo Fisher Scientific; 18418-012). qRT–PCR was performed with the Power SYBR green PCR master mix (Thermo Fisher Scientific; A25742) using a QuantStudio 3 Real-Time PCR System (Thermo Fisher Scientific). β-Actin was used for normalization of the assay, and fold change in expression was calculated by the $2^{-\Delta\Delta CT}$ method. The following primers were used for qRT-PCR:

D-loop mtDNA forward: 5'- CTATCACCCTATTAACCACTCA -3'

D-loop mtDNA reverse: 5'- TTCGCCTGTAATATTGAACGTA -3'

IFN-β forward: 5'- TGCTCTCCTGTTGTGCTTCTCCAC -3'

IFN-β reverse: 5'- ATAGATGGTCAATGCGGCGTCC-3'

Beta-Actin forward: 5'- TGCCATCCTAAAAGCCACCCCACTTC -3'

Beta-Actin reverse: 5'- AAGCAATGCTATCACCTCCCCTGTGT -3'

Transmission electron microscopy

Cells were seeded in 60 mm cell culture-treated dishes (Thermo Fisher Scientific; 174888) pre-coated with poly-L-Lysine. The cells were gently washed with PBS and fixed with a mixture of 2.5% glutaraldehyde and 2% paraformaldehyde in 0.1 M phosphate buffer (pH 7.4). The samples were then fixed in 1% osmium tetroxide in 0.1 M phosphate buffer (pH 7.4) for 1 h. The samples were dehydrated using a graded ethanol series, followed by acetone, and were embedded in LX-112 (Ladd Research, Williston, VT). Thin sections (65 nm) were stained with uranyl acetate and lead citrate. Imaging was performed using a JEOL JEM1400 Transmission Electron Microscope (JEOL USA Inc., Peabody, MA, USA) at the Penn State College of Medicine TEM Facility (RRID Number: SCR_021200).

Statistical analysis

Data are presented as mean ± standard deviation relative to the control from a representative experiment with triplicate samples. Statistical analysis was performed using GraphPad Prism 10.1.2 and indicated in the figure legends and supplemental figure legends.

Acknowledgements

The authors thank Dr. Richard Youle (National Institutes of Health) for HeLa pentaKO cells; Dr. Warner Greene (University of California San Francisco) for Jurkat Tax and Tax M22 Tet-On cells; Dr. Wen-Xing Ding (University of Kansas Medical Center) for HeLa LC3-GFP cells; Dr. Lee Ratner (Washington University) for the pACH proviral clone plasmid and Dr. Aleem Siddiqui (University of California San Diego) for the GFP-RFP-Mito reporter plasmid. We are grateful to the HAM/TSP patients who contributed to this study. We thank Dr. Han Chen for assistance with TEM studies. This work was supported by NIH grants R21 AI166335 and R01 AI162815 (to EWH) and the NINDS intramural research program (S.J.). The experiments in this manuscript used the Penn State College of Medicine Advanced Light Microscopy Core, TEM Core and the Flow Cytometry Core. The Advanced Light Microscopy Core (RRID: SCR_022526), the TEM Core (RRID:SCR_021200) and Flow Cytometry Core (RRID:SCR_021134), services and instruments used in this project were funded, in part, by the Pennsylvania State University College of Medicine via the Office of the Vice Dean of Research and Graduate Students and the Pennsylvania Department of Health using Tobacco Settlement Funds (CURE). The content is solely the responsibility of the authors and does not necessarily represent the official views of the University or College of Medicine. The Pennsylvania Department of Health specifically disclaims responsibility for any analyses, interpretations, or conclusions.

Author Contributions Statement

S.M., S.S. and E.W.H. designed the experiments. S.M. and S.S. performed all of the experiments. S.M., S.S., N.M. and E.W.H. analyzed the data. S.J. provided HAM/TSP patient PBMCs. S.M. and E.W.H. wrote the manuscript. S.S., S.M., N.M., S.J. and E.W.H. edited the manuscript. E.W.H.

conceived and supervised the project and acquired funding for the project. All authors reviewed and approved the manuscript.

Ethics Declarations

The authors declare no competing interests.

Data availability

All data are available in the main text or supplementary materials.

FIGURE 1

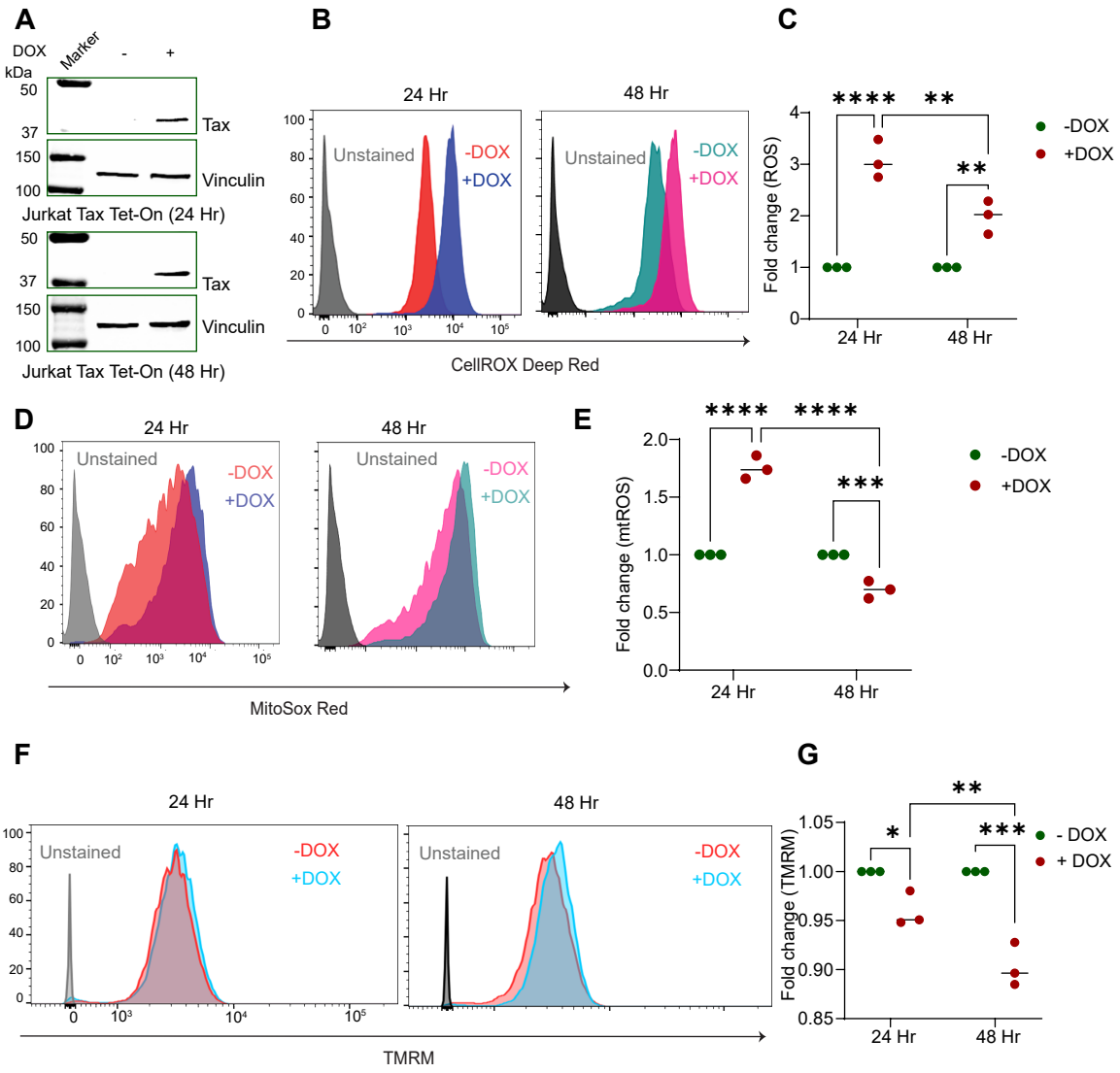

710

Fig. 1. Tax expression is associated with dynamic changes in mitochondrial ROS and membrane potential. A. Immunoblotting was performed with the indicated antibodies using lysates from Jurkat Tax Tet-On cells treated with 1 μg/ml DOX for 24 and 48 h. Data are representative of three independent experiments with similar results. Protein levels were normalized to the loading control (vinculin) and compared to the untreated control. **B.** Jurkat Tax Tet-On cells were treated with DOX for the indicated time points and stained with CellROX Deep Red for the detection of ROS by flow cytometry. **C.** Graphical representation indicating the fold change in ROS levels in three biological replicates compared to untreated controls. The results are expressed as the mean ± SD of three independent experiments. $****P < 0.0001$; $**P < 0.01$. Two-way ANOVA with Tukey's multiple comparisons test. **D.** Jurkat Tax Tet-On cells were treated with DOX for the indicated time points and stained with mitoSOX Red for the detection of mtROS by flow cytometry. **E.** Graphical representation indicating the fold change in mtROS levels in three biological replicates compared to untreated controls. The results are expressed as the mean ± SD of three independent experiments. $****P < 0.0001$; $***P < 0.001$. Two-way ANOVA with multiple comparisons test. **F.** Jurkat Tax Tet-On cells were treated with DOX for the indicated time points and stained with TMRM to assess mitochondrial membrane potential by flow cytometry. **G.** Graphical representation indicating the fold change in mitochondrial membrane potential in three biological replicates compared to untreated controls. The results are expressed as the mean ± SD of three independent experiments. $***P < 0.001$; $**P < 0.01$; $*P < 0.05$. Two-way ANOVA with multiple comparisons test.

FIGURE 2

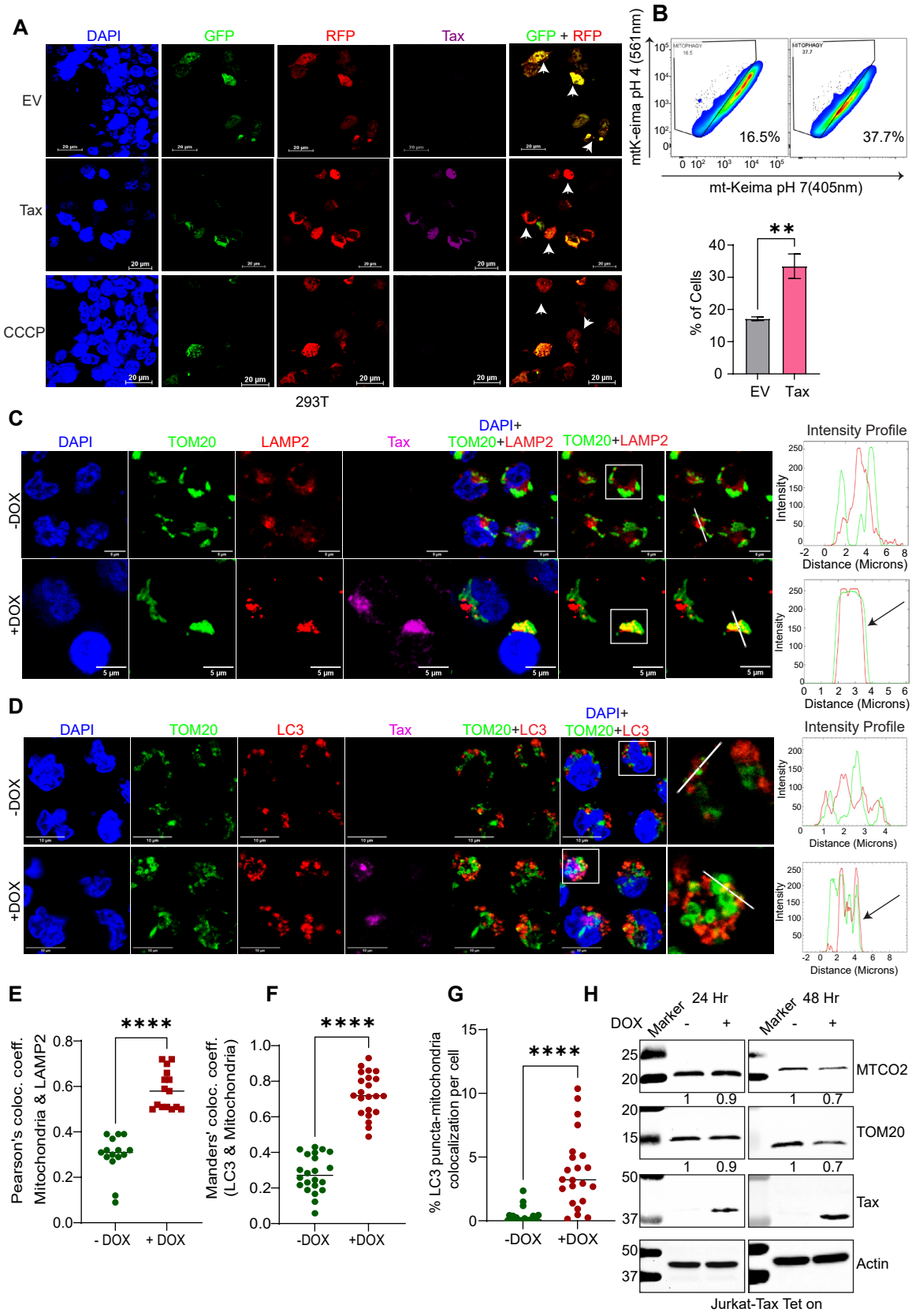

Fig. 2. Tax induces complete mitophagy. A. Immunofluorescence confocal microscopy was performed using 293T cells transfected with a GFP-RFP-Mito reporter and either an empty vector (EV) or Tax. CCCP treatment (4 h) was used as a positive control for mitophagy induction. **B.** Flow cytometric analysis of mt-Keima fluorescence in 293T cells transfected with EV or Tax and the mt-mKeima plasmid. The graph indicates the percentage of cells with a pH 4 shift (mitophagy). Unpaired Student's *t* test, $^{**}P < 0.01$. **C.** Immunofluorescence confocal microscopy was performed using Jurkat Tax Tet-On cells either untreated or treated with DOX (48 h) and leupeptin (20 µM). Cells were labeled with TOM20-CoraLite® Plus 488 (mitochondria), LAMP2-Alexa Fluor 647 (lysosomes, pseudo-red) and Tax-Alexa Fluor 594 (pseudo-magenta) antibodies and DAPI (nucleus). The overlap in intensity profiles (Fiji) indicates TOM20 and LAMP2 colocalization. **D.** Immunofluorescence confocal microscopy was performed using Jurkat Tax Tet-On cells either untreated or treated with DOX (48 h) and BafA1 (20 nM). Cells were labeled with TOM20-CoraLite® Plus 488 (mitochondria), LC3-Alexa Fluor 594 (autophagosomes) and Tax-Alexa Fluor 647 antibodies and DAPI. The overlap in intensity profiles (Fiji) indicates TOM20 and LC3 colocalization. **E.** Pearson's colocalization coefficient for LAMP2 and TOM20 in Jurkat Tax Tet-On cells ± DOX and leupeptin (Fiji/COLOC2) where each dot represents a single cell (n=15 cells). The results are expressed as the mean ± SD. Unpaired Student's *t* test with Welch's correction. $^{****}P < 0.0001$. **F.** Manders' colocalization coefficient for LC3 and TOM20 in Jurkat Tax Tet-On cells ± DOX and BAF A1 (Fiji/JACOP), (n=22 cells). Unpaired Student's *t* test with Welch's correction. $^{****}P < 0.0001$. **G.** Graphical representation indicating the percentage of LC3 puncta colocalized with mitochondria (TOM20), (n=22 cells). Unpaired Student's *t* test with Welch's correction. $^{****}P < 0.0001$. **H.** Immunoblotting was performed with the indicated antibodies using lysates from Jurkat Tax Tet-On cells either untreated or treated with DOX at the indicated time points. Protein levels were normalized to the loading control (Actin) and compared to untreated Jurkat-Tax Tet-On cells. Data are representative of three independent experiments with similar results.

FIGURE 3

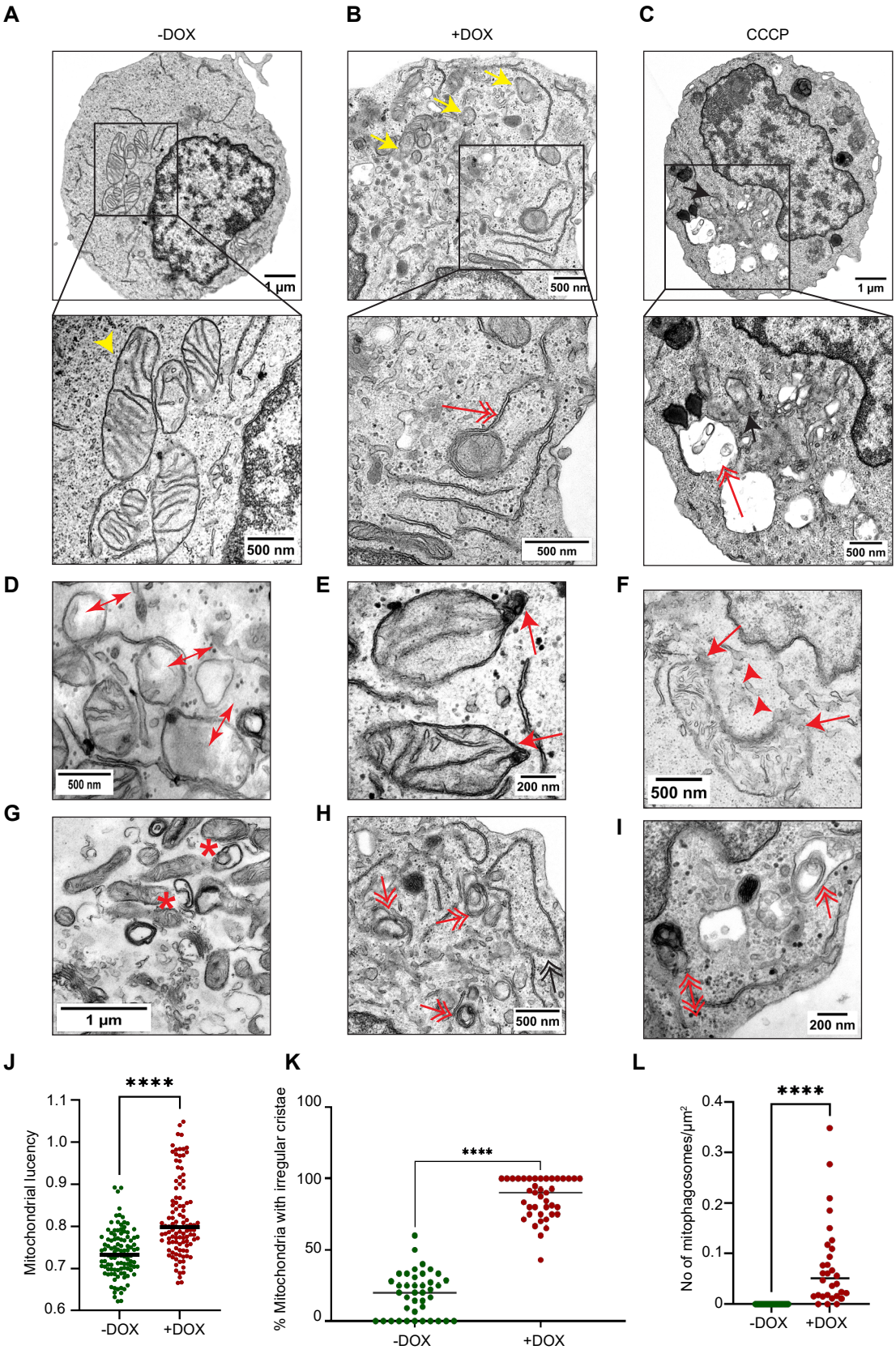

Fig. 3. Tax expression causes dramatic changes in mitochondrial ultrastructure. A. Transmission electron microscopy (TEM) images of untreated Jurkat Tax Tet-On cells reveal healthy mitochondria with well-defined cristae and a tubular shape (yellow arrowhead). **B.** TEM images of DOX-treated Jurkat Tax Tet-On cells reveal damaged mitochondria (yellow arrow) with irregular cristae and mitophagosomes (double-headed red arrow). **C.** TEM images of CCCP-treated Jurkat Tax Tet-On cells display abnormal mitochondria (black arrow) with irregular cristae and mitophagosomes (double-headed red arrow). **D.** TEM image showing high-translucency mitochondria with irregular cristae (double-sided arrow) in DOX-treated Jurkat Tax Tet-On cells. **E.** TEM image of DOX-treated Jurkat Tax Tet-On cells showing swollen and ruptured outer mitochondrial membrane (red arrow). **F.** TEM image of mitochondria with irregular cristae and leakage of mitochondrial content into the cytoplasm (red arrowhead) in DOX-treated Jurkat Tax Tet-On cells. **G.** TEM image showing early autophagophores (star shape) adjacent to damaged mitochondria in DOX-treated Jurkat Tax Tet-On cells. **H.** TEM image of multiple mitophagosomes (double-headed red arrow) in DOX-treated Jurkat Tax Tet-On cells. **I.** TEM image showing mitophagosomes and late mitophagosomes/heterolysosomes (double-headed double-sided red arrow) in DOX-treated Jurkat Tax Tet-On cells. **J.** Graphical representation of the lucency of individual mitochondria in Jurkat Tax Tet-On cells, normalized to the lucency of the cytoplasm within individual cells (to adjust the brightness of each sample) of untreated and DOX-treated cells, where each dot represents a single cell (n=107 cells). The results are expressed as the mean ± SD. Unpaired Student's *t* test with Welch's correction ****$P < 0.0001$. **K.** Quantification of the percentage of mitochondria with irregular cristae in untreated and DOX-treated Jurkat Tax Tet-On cells, where each dot represents a single cell (n=40 cells). The results are expressed as the mean ± SD. Unpaired Student's *t* test with Welch's correction, ****$P < 0.0001$. **L.** Quantification of the number of mitophagosomes, normalized to the area of individual cells in untreated and DOX-treated Jurkat Tax Tet-On cells, where each dot represents a single cell (n=30 cells). The results are expressed as the mean ± SD. Unpaired Student's *t* test with Welch's correction, ****$P < 0.0001$.

FIGURE 4

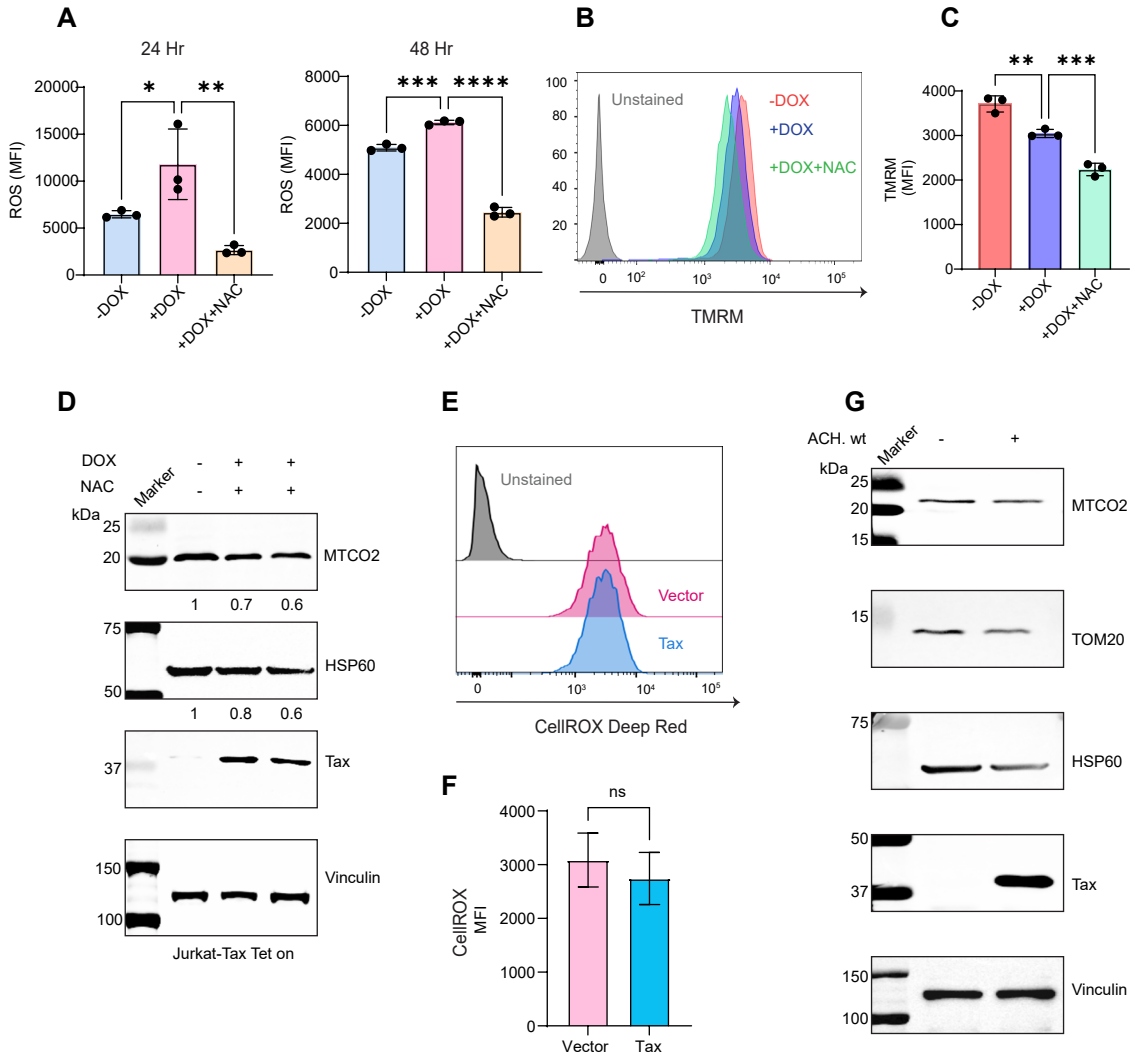

789

Fig. 4. Tax induction of mitophagy can occur in the absence of ROS. A. Graphical representation of ROS levels (MFI) measured by flow cytometric analysis of Jurkat Tax Tet-On cells that were untreated, treated with DOX alone or DOX and N-acetylcysteine (NAC, 20 mM) at the indicated time points and stained with CellROX Deep Red. The graph is based on three biological replicates and compared to untreated controls. $****P < 0.0001$; $***P < 0.001$; $**P < 0.01$; $*P < 0.05$. Ordinary one-way ANOVA with Šídák's multiple comparisons test. **B.** Jurkat Tax Tet-On cells were untreated, treated with DOX or DOX and NAC for 48 h and stained with TMRM to assess mitochondrial membrane potential by flow cytometry. **C.** Graphical representation of TMRM staining (MFI) of Jurkat Tax Tet-On cells as described in panel B, at 48 h, from three biological replicates compared to untreated controls. The results are expressed as the mean ± SD of three independent experiments. $***P < 0.001$; $**P < 0.01$. Ordinary one-way ANOVA with Šídák's multiple comparisons test. **D.** Immunoblotting was performed with the indicated antibodies using lysates from Jurkat Tax Tet-On cells treated with or without DOX and NAC for 48 h. Protein levels were normalized to the loading control (vinculin) and compared to untreated Jurkat-Tax Tet-On cells. Data are representative of three independent experiments with similar results. **E.** 293T cells transiently transfected with Tax were stained with CellROX Deep Red for the detection of ROS by flow cytometry. **F.** Graphical representation of ROS levels (MFI) in 293T cells transfected with Tax compared to EV controls, based on three biological replicates. Unpaired Student's *t* test, ns= not significant. **G.** Immunoblotting was performed with the indicated antibodies using lysates from 293T cells transfected with the ACH.WT HTLV-1 proviral clone. Protein levels were normalized to the loading control (vinculin) and compared to untransfected 293T cells.

FIGURE 5

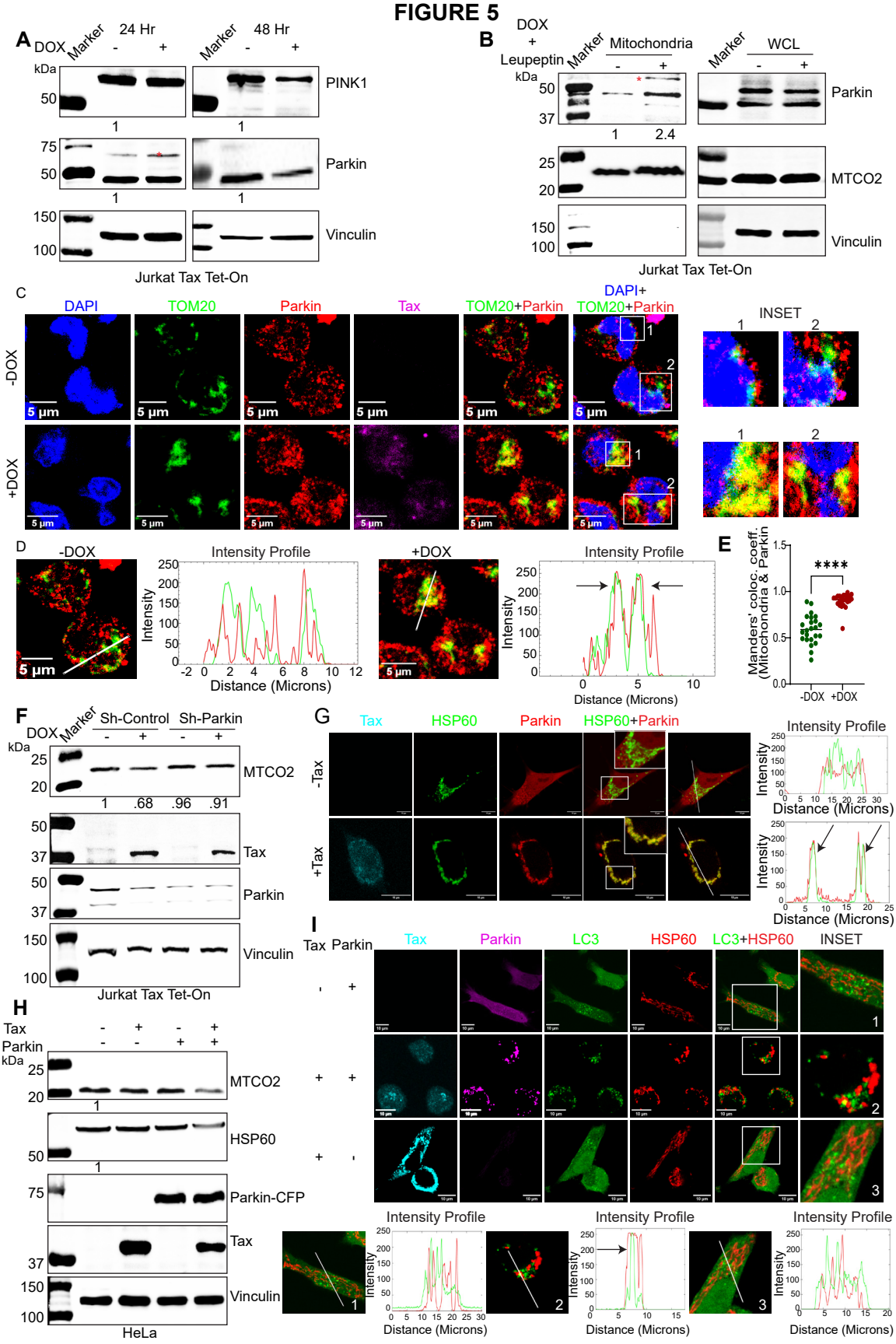

Fig 5. Tax induces Parkin-dependent mitophagy. A. Immunoblotting was performed with the indicated antibodies using lysates from untreated or DOX-treated Jurkat Tax Tet-On cells at the indicated time points. Data are representative of three independent experiments with similar results. Protein levels were normalized to the loading control (vinculin) and compared to untreated Jurkat-Tax Tet-On cells. **B.** Immunoblotting was performed with the indicated antibodies using mitochondrial fractions and whole cell lysates (WCL) from untreated or DOX and leupeptin-treated Jurkat Tax Tet-On cells for 48 h. Protein levels were normalized to the mitochondrial marker, MTCO2, and compared to untreated Jurkat-Tax Tet-On cells**. C.** Immunofluorescence confocal microscopy was performed using untreated or DOX and leupeptin-treated Jurkat Tax Tet-On cells for 48 h. Cells were labeled with TOM20-CoraLite® Plus 488 (mitochondria), Parkin-Alexa Fluor 594 and Tax-Alexa Fluor 647 antibodies and DAPI. Magnified views of TOM20 and Parkin overlap, highlighting colocalized areas in the zoomed-in sections of Jurkat Tax Tet-On cells (INSET). **D.** The overlap in intensity profiles (Fiji) indicates TOM20 and Parkin colocalization. **E.** Manders' colocalization coefficient for Parkin and TOM20 (mitochondria) from samples in panel C using the Fiji/JACOP plugin, where each dot represents a single cell (n=24 cells). The results are expressed as the mean ± SD. Unpaired Student's *t* test, $^{****}P < 0.0001$. **F.** Immunoblotting was performed with the indicated antibodies using lysates from untreated or DOX-treated (48 h) sh-Control and sh-Parkin Jurkat Tax Tet-On cells. Protein levels were normalized to the loading control (vinculin) and compared to untreated sh-Control Jurkat-Tax Tet-On cells. Data are representative of three independent experiments with similar results. **G.** Immunofluorescence confocal microscopy was performed with HeLa cells transfected with EV or Tax together with Parkin-mCherry and labeled with HSP60-Alexa Fluor 488 (mitochondria) and Tax-Alexa Fluor 405 (cyan) antibodies. The overlap in intensity profiles (Fiji) indicates HSP60 and Parkin colocalization. **H.** Immunoblotting was performed with the indicated antibodies using lysates from HeLa cells transfected with Tax and Parkin plasmids. Protein levels were normalized to the loading control (vinculin) and compared to transfected control. **I.** Immunofluorescence confocal microscopy was performed with HeLa LC3-GFP stable cells transfected with Tax and Parkin plasmids and labeled with HSP60-Alexa Fluor 647 (mitochondria, pseudo red) and Tax-Alexa Fluor 405 (cyan) antibodies. Parkin-mCherry was visualized in pseudo red using Fiji software. Magnified views of HSP60 and LC3 overlap, highlighting colocalized areas in the zoomed-in sections of HeLa LC3-GFP cells (INSET). Intensity profile analysis with Fiji software shows the overlap of HSP60 and LC3.

FIGURE 6

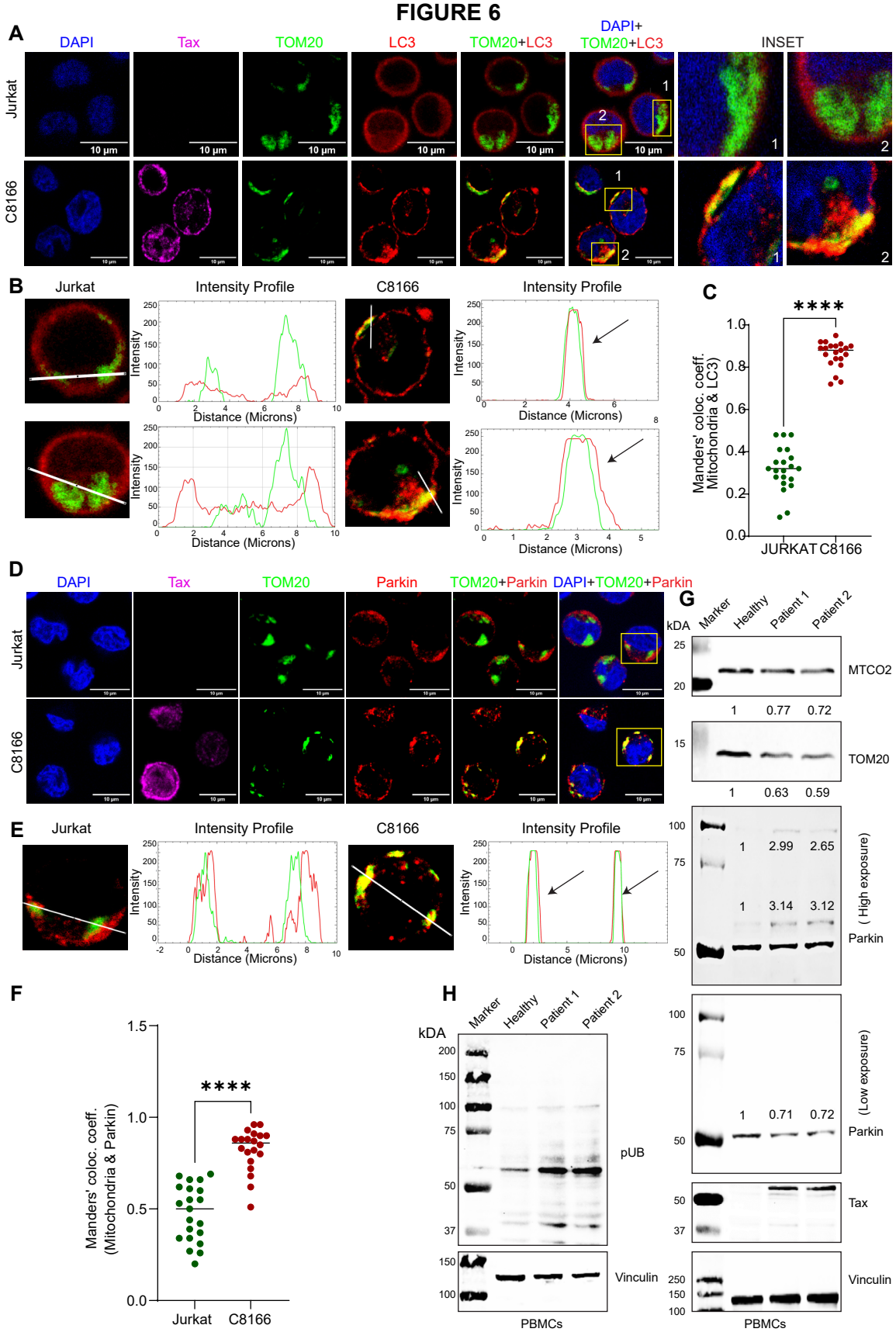

Fig. 6. Tax induces chronic Parkin-dependent mitophagy in HTLV-1 transformed cells and PBMCs from HAM/TSP patients. A. Immunofluorescence confocal microscopy was performed using Jurkat and C8166 cells labeled with TOM20-CoraLite® Plus 488 (mitochondria), LC3-Alexa Fluor 594 and Tax-Alexa Fluor 647 antibodies and DAPI. Magnified views of TOM20 and LC3 overlap, highlighting colocalized areas in the zoomed-in sections of Jurkat and C8166 cells (INSET). **B.** Intensity profile analysis with Fiji software shows the overlap between TOM20 and LC3. **C.** Manders' colocalization coefficient for TOM20 (mitochondria) and LC3 in C8166 and Jurkat cells using the Fiji/JACOP plugin, where each dot represents a single cell (n=21 cells). The results are expressed as the mean ± SD. Unpaired Student's *t* test, $****P < 0.0001$. **D.** Immunofluorescence confocal microscopy was performed using Jurkat and C8166 cells labeled with TOM20-CoraLite® Plus 488 (mitochondria), Parkin-Alexa Fluor 594 and Tax-Alexa Fluor 647 antibodies and DAPI. Magnified views of TOM20 and Parkin overlap, highlighting colocalized areas in the zoomed-in sections of Jurkat and C8166 cells (INSET). **E.** Intensity profile analysis from panel D using Fiji software, illustrating the overlap between TOM20 and Parkin. **F.** Manders' colocalization coefficient for TOM20 (mitochondria) and Parkin in C8166 and Jurkat cells using the Fiji/JACOP plugin, where each dot represents a single cell (n=21 cells). The results are expressed as the mean ± SD. Unpaired Student's *t* test, $****P < 0.0001$. **G, H.** Immunoblotting was performed with the indicated antibodies using lysates from control and HAM/TSP PBMCs. Protein levels were normalized to the loading control (vinculin) and was compared to control PBMCs.

FIGURE 7

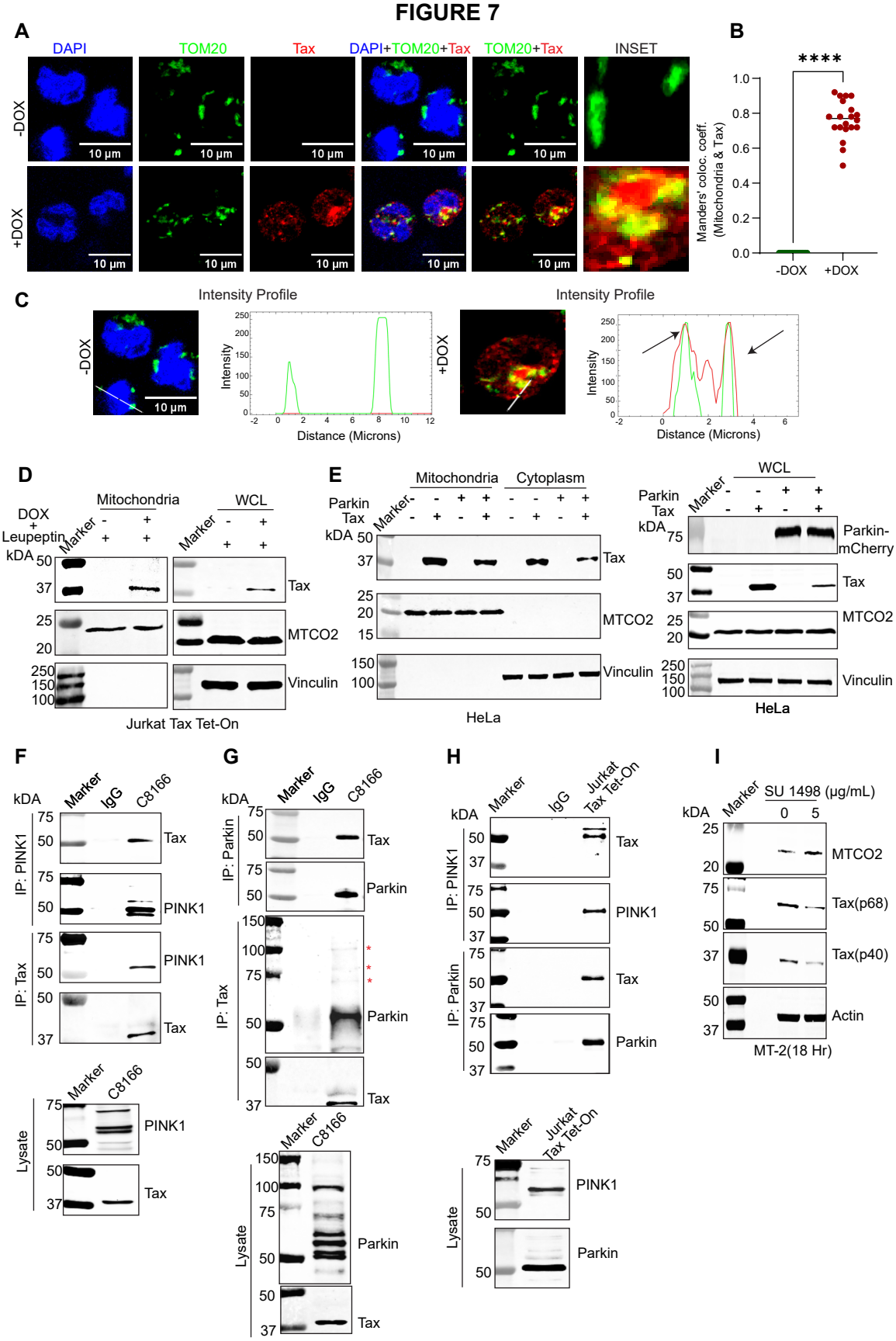

Fig. 7. Tax localizes to mitochondria and interacts with PINK1 and Parkin. A. Immunofluorescence confocal microscopy was performed using untreated or DOX and BafA1-treated (48 h) Jurkat Tax Tet-On cells. Cells were labeled with TOM20-CoraLite® Plus 488 (mitochondria) and Tax-Alexa Fluor 594 antibodies and DAPI. Magnified views of TOM20 and Tax overlap, highlighting areas of colocalization, shown in the zoomed-in sections of Jurkat Tax Tet-On cells (INSET). **B.** Manders' colocalization coefficient for TOM20 (mitochondria) and Tax in Jurkat Tax Tet-On cells using the Fiji/JACOP plugin, where each dot represents a single cell (n=20 cells). The results are expressed as the mean ± SD. Unpaired Student's *t* test, ****$P < 0.0001$. **C.** Intensity profile analysis from panel A using Fiji software, illustrating the overlap between TOM20 and Tax. **D.** Immunoblotting was performed with the indicated antibodies using mitochondrial fractions and WCL from untreated and DOX and leupeptin-treated (48 h) Jurkat Tax Tet-On cells **E.** Immunoblotting was performed with the indicated antibodies using mitochondrial fractions and WCL from HeLa cells transfected with the indicated plasmids. **F.** Co-IP assay was performed with either control IgG, PINK1 or Tax immunoprecipitates from lysates of C8166 cells. Immunoblotting was performed with lysates using the indicated antibodies. **G.** Co-IP assay was performed with either control IgG, Parkin or Tax immunoprecipitates from lysates of C8166 cells. Immunoblotting was performed with lysates using the indicated antibodies. **H.** Co-IP assay was performed with either control IgG, PINK1 or Parkin immunoprecipitates from lysates of DOX-treated Jurkat Tax Tet-On cells. Immunoblotting was performed with lysates using the indicated antibodies. **I.** Immunoblotting was performed with the indicated antibodies using lysates from SU 1498-treated (18 h) MT-2 cells.

FIGURE 8

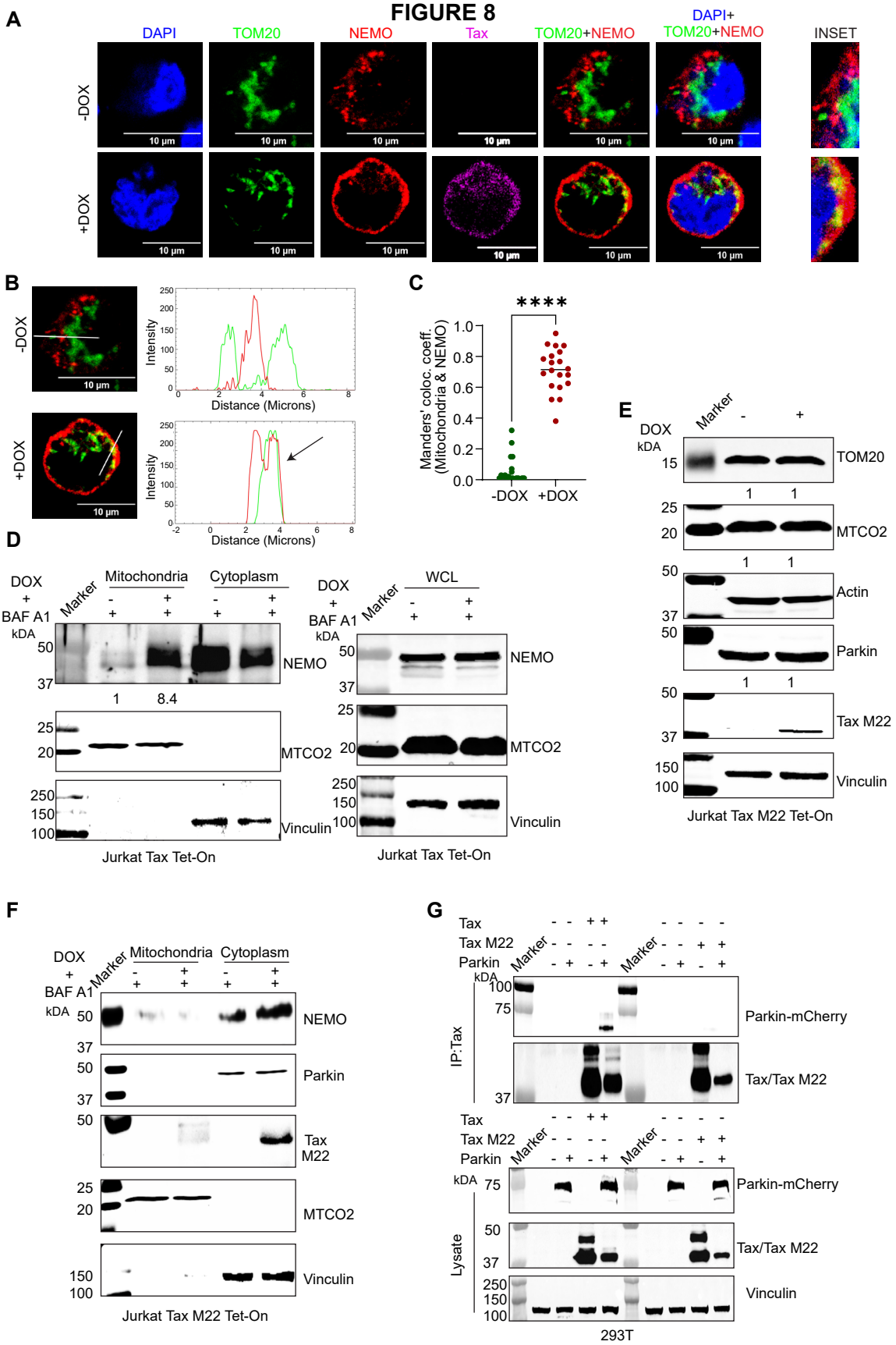

Fig. 8. The recruitment of NEMO to mitochondria is essential for Tax-induced mitophagy. **A.** Immunofluorescence confocal microscopy was performed using untreated or DOX and BafA1-treated (48 h) Jurkat Tax Tet-On cells. Cells were labeled with TOM20-CoraLite® Plus 488 (mitochondria), NEMO-Alexa Fluor 594 and Tax-Alexa Fluor 647 antibodies and DAPI. Magnified views of TOM20 and NEMO overlap, highlighting areas of colocalization, shown in the zoomed-in sections of Jurkat Tax Tet-On cells (INSET). **B.** Intensity profile analysis from panel A using Fiji software, illustrating the overlap between TOM20 and NEMO. **C.** Manders' colocalization coefficient for TOM20 (mitochondria) and NEMO in Jurkat Tax Tet-On cells using the Fiji/JACOP plugin, where each dot represents a single cell (n=20 cells). The results are expressed as the mean ± SD. Unpaired Student's *t* test, $****P < 0.0001$. **D.** Immunoblotting was performed with the indicated antibodies using mitochondrial fractions and WCL from untreated or DOX and BafA1-treated (48 h) Jurkat Tax Tet-On cells. Protein levels were normalized to the mitochondrial protein MTCO2 as the loading control and compared to untreated Jurkat Tax Tet-On cells. **E.** Immunoblotting was performed with the indicated antibodies using lysates from untreated or DOX-treated Jurkat-Tax M22 Tet-On cells. Protein levels were normalized to the loading control (vinculin) and compared to untreated Jurkat-Tax M22 Tet-on cells. **F.** Immunoblotting was performed with the indicated antibodies using mitochondrial fractions and WCL from was performed with the indicated antibodies using Jurkat-Tax M22 Tet-on cells. **G.** Co-IP assay was performed with either Parkin, Tax or Tax M22 immunoprecipitates from lysates of 293T cells transfected with Tax, Tax M22 and Parkin. Immunoblotting was performed with lysates using the indicated antibodies.

FIGURE 9

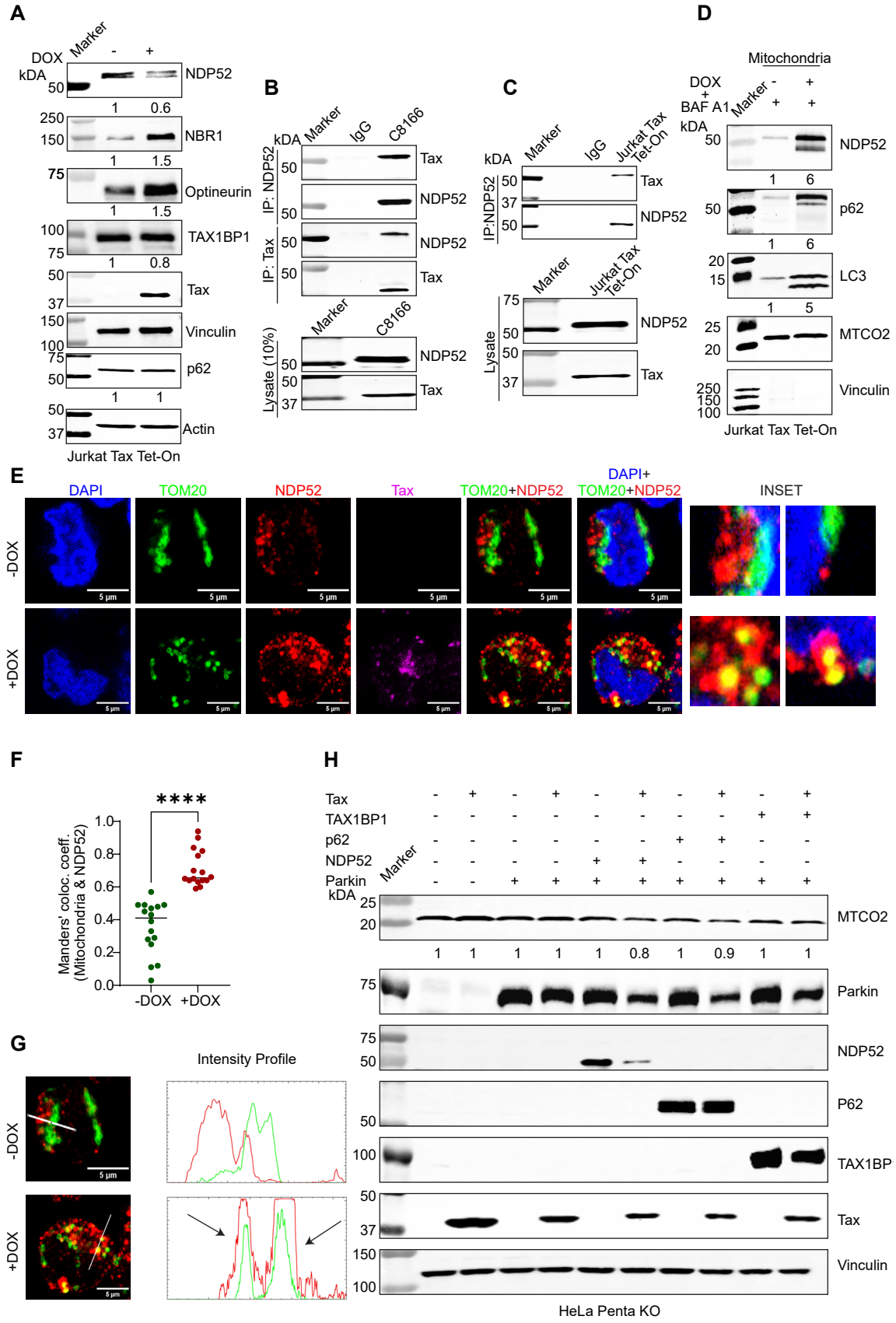

Fig. 9. Tax interacts with and recruits NDP52 to damaged mitochondria. A. Immunoblotting was performed with the indicated antibodies using lysates from untreated or DOX-treated (48 h) Jurkat Tax Tet-On cells. Protein levels were normalized to loading controls (Vinculin and Actin) and compared to untreated Jurkat Tax Tet-On cells. **B, C.** Co-IP assay was performed with either control IgG, NDP52 or Tax immunoprecipitates from lysates of C8166 cells (B) or DOX-treated Jurkat Tax Tet-On cells (C). Immunoblotting was performed with lysates using the indicated antibodies. **D.** Immunoblotting was performed with the indicated antibodies using mitochondrial fractions and WCL from untreated or DOX and BafA1-treated (48 h) Jurkat Tax Tet-On cells. **E.** Immunofluorescence confocal microscopy was performed using untreated or DOX and BafA1-treated (48 h) Jurkat Tax Tet-On cells. Cells were labeled with TOM20-CoraLite® Plus 488 (mitochondria), NDP52-Alexa Fluor 594 and Tax-Alexa Fluor 647 antibodies and DAPI. Magnified views of TOM20 and NDP52 overlap, highlighting areas of colocalization, shown in the zoomed-in sections of Jurkat Tax Tet-On cells (INSET). **F.** Manders' colocalization coefficient for TOM20 (mitochondria) and NDP52 in Jurkat Tax Tet-On cells using the Fiji/JACOP plugin, where each dot represents a single cell (n=16 cells). The results are expressed as the mean ± SD. Unpaired Student's *t* test, $****P < 0.0001$. **G.** Intensity profile analysis from panel E using Fiji software, illustrating the overlap between TOM20 and NDP52. **H.** Immunoblotting was performed with the indicated antibodies using lysates from HeLa PentaKO cells transfected with the indicated plasmids. MTCO2 protein levels were normalized to loading controls (vinculin) and compared to untransfected cells.

FIGURE 10

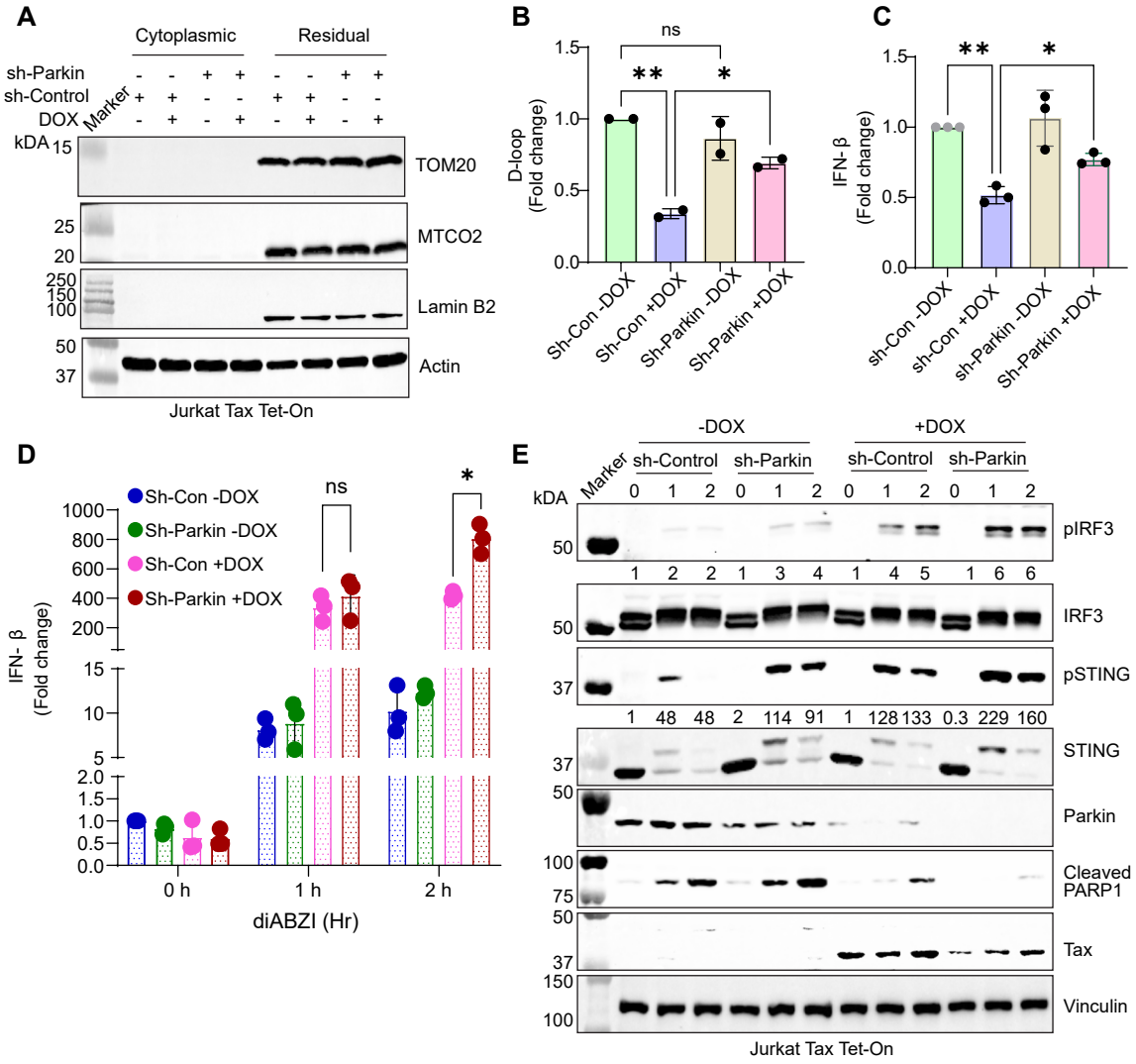

Fig. 10. Tax triggers mitophagy to limit cGAS-STING activation and type I IFN induction. **A.** Immunoblotting was performed with the indicated antibodies using cytoplasmic and residual fractions from untreated or DOX-treated Jurkat Tax Tet-On cells. **B.** qRT-PCR of D-loop mRNA in untreated or DOX-treated sh-Control and sh-Parkin Jurkat Tax Tet-On cells. The results are expressed as the mean ± SD of three independent experiments. $^{**}P < 0.01$; $^{*}P < 0.05$; ns=not significant. Ordinary one-way ANOVA with Šídák's multiple comparisons test. **C.** qRT-PCR of *Ifnb* mRNA in untreated or DOX-treated sh-Control and sh-Parkin Jurkat Tax Tet-On cells. The results are expressed as the mean ± SD of three independent experiments. $^{**}P < 0.01$; $^{*}P < 0.05$. Ordinary one-way ANOVA with Šídák's multiple comparisons test **D.** qRT-PCR of *Ifnb* mRNA in untreated or DOX-treated sh-Control and sh-Parkin Jurkat Tax Tet-On cells treated with diABZI (1 μM) for the indicated times. The results are expressed as the mean ± SD of three independent experiments. $^{*}P < 0.05$; ns=not significant. Two-way ANOVA with Tukey's multiple comparisons test. **E.** Immunoblotting was performed with the indicated antibodies using lysates from untreated or DOX-treated (48 h) sh-Control and sh-Parkin Jurkat Tax Tet-On cells treated with diABZI (1 μM) for the indicated times. Protein levels were normalized to loading controls (vinculin) and compared to untreated sh-Control Jurkat Tax Tet-On cells. **F.** Model depicting HTLV-1 Tax induction of mitophagy. Tax induces ROS and mitochondrial dysfunction and is recruited to damaged mitochondria through binding to NEMO. Tax interacts with PINK1, Parkin and NDP52 to promote mitophagy, facilitating the removal of damaged mitochondria. Tax-triggered mitophagy limits the extent of cGAS-STING activation and type I IFN induction. The schematic was created with BioRender.com and released under a Creative Commons Attribution-NonCommercial-NoDerivs 4.0 International license.

References

1. Gessain, A. & Cassar, O. Epidemiological Aspects and World Distribution of HTLV-1 Infection. *Frontiers in microbiology* **3**, 388 (2012).
2. Phillips, A.A. & Harewood, J.C.K. Adult T Cell Leukemia-Lymphoma (ATL): State of the Art. *Current hematologic malignancy reports* **13**, 300-307 (2018).
3. Levin, M.C. & Jacobson, S. HTLV-I associated myelopathy/tropical spastic paraparesis (HAM/TSP): a chronic progressive neurologic disease associated with immunologically mediated damage to the central nervous system. *J Neurovirol* **3**, 126-140 (1997).
4. Phillips, A.A. Advances in the treatment of HTLV-1-associated adult T-cell leukemia lymphoma. *Curr Opin Virol* **58**, 101289 (2023).
5. Mohanty, S. & Harhaj, E.W. Mechanisms of Oncogenesis by HTLV-1 Tax. *Pathogens* **9** (2020).
6. Ma, G., Yasunaga, J. & Matsuoka, M. Multifaceted functions and roles of HBZ in HTLV-1 pathogenesis. *Retrovirology* **13**, 16 (2016).
7. Hyun, J. *et al.* Oncogenic human T-cell lymphotropic virus type 1 tax suppression of primary innate immune signaling pathways. *J Virol* **89**, 4880-4893 (2015).
8. Wang, J., Yang, S., Liu, L., Wang, H. & Yang, B. HTLV-1 Tax impairs K63-linked ubiquitination of STING to evade host innate immunity. *Virus Res* **232**, 13-21 (2017).
9. Mohanty, S. & Harhaj, E.W. Mechanisms of Innate Immune Sensing of HTLV-1 and Viral Immune Evasion. *Pathogens* **12** (2023).
10. Kulkarni, A. & Bangham, C.R.M. HTLV-1: Regulating the Balance Between Proviral Latency and Reactivation. *Frontiers in microbiology* **9**, 449 (2018).
11. Kulkarni, A., Taylor, G.P., Klose, R.J., Schofield, C.J. & Bangham, C.R. Histone H2A monoubiquitylation and p38-MAPKs regulate immediate-early gene-like reactivation of latent retrovirus HTLV-1. *JCI Insight* **3** (2018).
12. Mahgoub, M. *et al.* Sporadic on/off switching of HTLV-1 Tax expression is crucial to maintain the whole population of virus-induced leukemic cells. *Proc Natl Acad Sci U S A* (2018).
13. Harhaj, E.W. & Giam, C.Z. NF-kappaB signaling mechanisms in HTLV-1-induced adult T-cell leukemia/lymphoma. *FEBS J* **285**, 3324-3336 (2018).
14. Tang, S.W., Chen, C.Y., Klase, Z., Zane, L. & Jeang, K.T. The cellular autophagy pathway modulates human T-cell leukemia virus type 1 replication. *J Virol* **87**, 1699-1707 (2013).
15. Wang, W. *et al.* Human T-cell leukemia virus type 1 Tax-deregulated autophagy pathway and c-FLIP expression contribute to resistance against death receptor-mediated apoptosis. *J Virol* **88**, 2786-2798 (2014).
16. Ducasa, N. *et al.* Autophagy in Human T-Cell Leukemia Virus Type 1 (HTLV-1) Induced Leukemia. *Front Oncol* **11**, 641269 (2021).
17. Ren, T. *et al.* HTLV-1 Tax deregulates autophagy by recruiting autophagic molecules into lipid raft microdomains. *Oncogene* **34**, 334-345 (2015).
18. Chen, L., Liu, D., Zhang, Y., Zhang, H. & Cheng, H. The autophagy molecule Beclin 1 maintains persistent activity of NF-kappaB and Stat3 in HTLV-1-transformed T lymphocytes. *Biochem Biophys Res Commun* **465**, 739-745 (2015).
19. Kinjo, T., Ham-Terhune, J., Peloponese, J.M., Jr. & Jeang, K.T. Induction of reactive oxygen species by human T-cell leukemia virus type 1 tax correlates with DNA damage and expression of cellular senescence marker. *J Virol* **84**, 5431-5437 (2010).

20. Takahashi, M. *et al.* HTLV-1 Tax oncoprotein stimulates ROS production and apoptosis in T cells by interacting with USP10. *Blood* **122**, 715-725 (2013).
21. Choi, Y.B. & Harhaj, E.W. HTLV-1 tax stabilizes MCL-1 via TRAF6-dependent K63-linked polyubiquitination to promote cell survival and transformation. *PLoS Pathog* **10**, e1004458 (2014).
22. Gao, L. & Harhaj, E.W. HSP90 protects the human T-cell leukemia virus type 1 (HTLV-1) tax oncoprotein from proteasomal degradation to support NF-kappaB activation and HTLV-1 replication. *J Virol* **87**, 13640-13654 (2013).
23. Bock, F.J. & Tait, S.W.G. Mitochondria as multifaceted regulators of cell death. *Nat Rev Mol Cell Biol* **21**, 85-100 (2020).
24. Chen, W., Zhao, H. & Li, Y. Mitochondrial dynamics in health and disease: mechanisms and potential targets. *Signal Transduct Target Ther* **8**, 333 (2023).
25. Li, X. *et al.* Viral Infection Modulates Mitochondrial Function. *Int J Mol Sci* **22** (2021).
26. Sun, Z., Wang, Y., Jin, X., Li, S. & Qiu, H.J. Crosstalk between Dysfunctional Mitochondria and Proinflammatory Responses during Viral Infections. *Int J Mol Sci* **25** (2024).
27. Sorouri, M., Chang, T. & Hancks, D.C. Mitochondria and Viral Infection: Advances and Emerging Battlefronts. *mBio* **13**, e0209621 (2022).
28. Ge, P., Dawson, V.L. & Dawson, T.M. PINK1 and Parkin mitochondrial quality control: a source of regional vulnerability in Parkinson's disease. *Mol Neurodegener* **15**, 20 (2020).
29. Narendra, D.P. *et al.* PINK1 is selectively stabilized on impaired mitochondria to activate Parkin. *PLoS Biol* **8**, e1000298 (2010).
30. Matsuda, N. *et al.* PINK1 stabilized by mitochondrial depolarization recruits Parkin to damaged mitochondria and activates latent Parkin for mitophagy. *J Cell Biol* **189**, 211-221 (2010).
31. Narendra, D., Tanaka, A., Suen, D.F. & Youle, R.J. Parkin is recruited selectively to impaired mitochondria and promotes their autophagy. *J Cell Biol* **183**, 795-803 (2008).
32. Gegg, M.E. *et al.* Mitofusin 1 and mitofusin 2 are ubiquitinated in a PINK1/parkin-dependent manner upon induction of mitophagy. *Hum Mol Genet* **19**, 4861-4870 (2010).
33. Geisler, S. *et al.* PINK1/Parkin-mediated mitophagy is dependent on VDAC1 and p62/SQSTM1. *Nat Cell Biol* **12**, 119-131 (2010).
34. Sarraf, S.A. *et al.* Landscape of the PARKIN-dependent ubiquitylome in response to mitochondrial depolarization. *Nature* **496**, 372-376 (2013).
35. Harper, J.W., Ordureau, A. & Heo, J.M. Building and decoding ubiquitin chains for mitophagy. *Nat Rev Mol Cell Biol* **19**, 93-108 (2018).
36. Wang, S. *et al.* The mitophagy pathway and its implications in human diseases. *Signal Transduct Target Ther* **8**, 304 (2023).
37. Lazarou, M. *et al.* The ubiquitin kinase PINK1 recruits autophagy receptors to induce mitophagy. *Nature* **524**, 309-314 (2015).
38. Vilmen, G. *et al.* BHRF1, a BCL2 viral homolog, disturbs mitochondrial dynamics and stimulates mitophagy to dampen type I IFN induction. *Autophagy* **17**, 1296-1315 (2021).
39. Zhang, B. *et al.* The nucleoprotein of influenza A virus inhibits the innate immune response by inducing mitophagy. *Autophagy* **19**, 1916-1933 (2023).
40. Zhang, L., Qin, Y. & Chen, M. Viral strategies for triggering and manipulating mitophagy. *Autophagy* **14**, 1665-1673 (2018).

41. Kim, S.J. *et al.* Hepatitis B virus disrupts mitochondrial dynamics: induces fission and mitophagy to attenuate apoptosis. *PLoS Pathog* **9**, e1003722 (2013).
42. Kim, S.J. *et al.* Hepatitis C virus triggers mitochondrial fission and attenuates apoptosis to promote viral persistence. *Proc Natl Acad Sci U S A* **111**, 6413-6418 (2014).
43. Sun, N. *et al.* A fluorescence-based imaging method to measure in vitro and in vivo mitophagy using mt-Keima. *Nat Protoc* **12**, 1576-1587 (2017).
44. Kim, S.J., Ahn, D.G., Syed, G.H. & Siddiqui, A. The essential role of mitochondrial dynamics in antiviral immunity. *Mitochondrion* **41**, 21-27 (2018).
45. Taguchi, N., Ishihara, N., Jofuku, A., Oka, T. & Mihara, K. Mitotic phosphorylation of dynamin-related GTPase Drp1 participates in mitochondrial fission. *J Biol Chem* **282**, 11521-11529 (2007).
46. Robek, M.D. & Ratner, L. Immortalization of CD4(+) and CD8(+) T lymphocytes by human T-cell leukemia virus type 1 Tax mutants expressed in a functional molecular clone. *J Virol* **73**, 4856-4865 (1999).
47. Kane, L.A. *et al.* PINK1 phosphorylates ubiquitin to activate Parkin E3 ubiquitin ligase activity. *J Cell Biol* **205**, 143-153 (2014).
48. Kazlauskaite, A. *et al.* Binding to serine 65-phosphorylated ubiquitin primes Parkin for optimal PINK1-dependent phosphorylation and activation. *EMBO Rep* **16**, 939-954 (2015).
49. Mohanty, S. *et al.* The tyrosine kinase KDR is essential for the survival of HTLV-1-infected T cells by stabilizing the Tax oncoprotein. *Nature communications* **15**, 5380 (2024).
50. Harding, O., Holzer, E., Riley, J.F., Martens, S. & Holzbaur, E.L.F. Damaged mitochondria recruit the effector NEMO to activate NF-kappaB signaling. *Mol Cell* **83**, 3188-3204 e3187 (2023).
51. Shembade, N., Harhaj, N.S., Yamamoto, M., Akira, S. & Harhaj, E.W. The human T-cell leukemia virus type 1 Tax oncoprotein requires the ubiquitin-conjugating enzyme Ubc13 for NF-kappaB activation. *J Virol* **81**, 13735-13742 (2007).
52. Schwob, A. *et al.* SQSTM-1/p62 potentiates HTLV-1 Tax-mediated NF-kappaB activation through its ubiquitin binding function. *Sci Rep* **9**, 16014 (2019).
53. Gachon, F. *et al.* CREB-2, a cellular CRE-dependent transcription repressor, functions in association with Tax as an activator of the human T-cell leukemia virus type 1 promoter. *J Virol* **72**, 8332-8337 (1998).
54. Aguirre, S. *et al.* Dengue virus NS2B protein targets cGAS for degradation and prevents mitochondrial DNA sensing during infection. *Nat Microbiol* **2**, 17037 (2017).
55. Hu, M.M. & Shu, H.B. Mitochondrial DNA-triggered innate immune response: mechanisms and diseases. *Cellular & molecular immunology* **20**, 1403-1412 (2023).
56. Larkin, B. *et al.* Cutting Edge: Activation of STING in T Cells Induces Type I IFN Responses and Cell Death. *J Immunol* **199**, 397-402 (2017).
57. Kuhl, N. *et al.* STING agonism turns human T cells into interferon-producing cells but impedes their functionality. *EMBO Rep* **24**, e55536 (2023).
58. Cockfield, J.A. & Schafer, Z.T. Antioxidant Defenses: A Context-Specific Vulnerability of Cancer Cells. *Cancers (Basel)* **11** (2019).
59. Li, Y. *et al.* The Role of Mitophagy in Viral Infection. *Cells* **11** (2022).
60. Huang, X.Y. *et al.* Hepatitis B Virus X protein elevates Parkin-mediated mitophagy through Lon Peptidase in starvation. *Exp Cell Res* **368**, 75-83 (2018).
61. Jassey, A. *et al.* Hepatitis C Virus Non-Structural Protein 5A (NS5A) Disrupts Mitochondrial Dynamics and Induces Mitophagy. *Cells* **8** (2019).

62. Oh, S.J. *et al.* Varicella zoster virus glycoprotein E facilitates PINK1/Parkin-mediated mitophagy to evade STING and MAVS-mediated antiviral innate immunity. *Cell Death Dis* **15**, 16 (2024).
63. Zong, S. *et al.* SARS-CoV-2 Nsp8 induces mitophagy by damaging mitochondria. *Virol Sin* **38**, 520-530 (2023).
64. Li, S. *et al.* Porcine reproductive and respiratory syndrome virus triggers mitochondrial fission and mitophagy to attenuate apoptosis. *Oncotarget* **7**, 56002-56012 (2016).
65. Kulkarni, A. *et al.* Glucose Metabolism and Oxygen Availability Govern Reactivation of the Latent Human Retrovirus HTLV-1. *Cell Chem Biol* **24**, 1377-1387 e1373 (2017).
66. Liu, Y. *et al.* Hypoxia-induced GPCPD1 depalmitoylation triggers mitophagy via regulating PRKN-mediated ubiquitination of VDAC1. *Autophagy* **19**, 2443-2463 (2023).
67. Harhaj, E.W. & Sun, S.C. IKKgamma serves as a docking subunit of the IkappaB kinase (IKK) and mediates interaction of IKK with the human T-cell leukemia virus Tax protein. *J Biol Chem* **274**, 22911-22914 (1999).
68. Kwon, H. *et al.* Lethal cutaneous disease in transgenic mice conditionally expressing type I human T cell leukemia virus Tax. *J Biol Chem* **280**, 35713-35722 (2005).
69. Kataura, T. *et al.* NDP52 acts as a redox sensor in PINK1/Parkin-mediated mitophagy. *EMBO J* **42**, e111372 (2023).
70. Aarreberg, L.D. *et al.* Interleukin-1beta Induces mtDNA Release to Activate Innate Immune Signaling via cGAS-STING. *Mol Cell* **74**, 801-815 e806 (2019).
71. Nakahira, K. *et al.* Autophagy proteins regulate innate immune responses by inhibiting the release of mitochondrial DNA mediated by the NALP3 inflammasome. *Nat Immunol* **12**, 222-230 (2011).
72. Liao, S., Chen, L., Song, Z. & He, H. The fate of damaged mitochondrial DNA in the cell. *Biochim Biophys Acta Mol Cell Res* **1869**, 119233 (2022).
73. Sliter, D.A. *et al.* Parkin and PINK1 mitigate STING-induced inflammation. *Nature* **561**, 258-262 (2018).
74. Harhaj, E.W., Good, L., Xiao, G. & Sun, S.C. Gene expression profiles in HTLV-I-immortalized T cells: deregulated expression of genes involved in apoptosis regulation. *Oncogene* **18**, 1341-1349 (1999).
75. Macaire, H. *et al.* Tax protein-induced expression of antiapoptotic Bfl-1 protein contributes to survival of human T-cell leukemia virus type 1 (HTLV-1)-infected T-cells. *J Biol Chem* **287**, 21357-21370 (2012).
76. Silic-Benussi, M. *et al.* HTLV-1 p13, a small protein with a busy agenda. *Mol Aspects Med* **31**, 350-358 (2010).
77. Hutchison, T. *et al.* The TP53-Induced Glycolysis and Apoptosis Regulator mediates cooperation between HTLV-1 p30(II) and the retroviral oncoproteins Tax and HBZ and is highly expressed in an in vivo xenograft model of HTLV-1-induced lymphoma. *Virology* **520**, 39-58 (2018).
78. Mohanty, S. *et al.* The E3/E4 ubiquitin conjugation factor UBE4B interacts with and ubiquitinates the HTLV-1 Tax oncoprotein to promote NF-kappaB activation. *PLoS Pathog* **16**, e1008504 (2020).

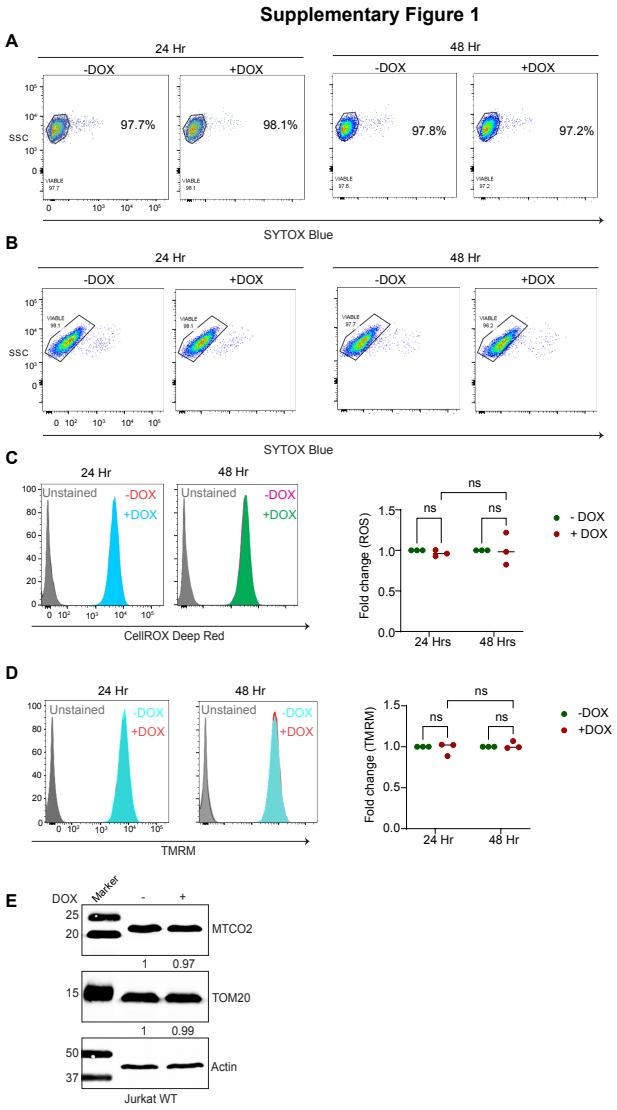

Supplementary Figure 1. DOX treatment does not induce mitochondrial damage in Jurkat cells. **(A, B)** Jurkat Tax Tet-On and Jurkat cells were treated with DOX for the indicated time points and stained with SYTOX Blue to assess cell viability. **(C)** Jurkat cells were treated with DOX for the indicated time points and stained with CellROX Deep Red for the detection of ROS by flow cytometry. Graphical representation indicating the fold change in ROS in three biological replicates compared to untreated controls. The results are expressed as the mean ± SD of three independent experiments. ns=not significant. Two-way ANOVA with Tukey's multiple comparisons test. **(D)** Jurkat cells were treated with DOX for the indicated time points and stained with TMRM to assess mitochondrial membrane potential by flow cytometry. Graphical representation indicating the fold change in mitochondrial membrane potential in three biological replicates compared to untreated controls. The results are expressed as the mean ± SD of three independent experiments. ns=not significant. Two-way ANOVA with multiple comparisons test. **(E)** Immunoblotting was performed with the indicated antibodies using lysates from Jurkat cells either untreated or treated with DOX for 48 h. Protein levels were normalized to the loading control (Actin) and compared to untreated Jurkat cells.

Supplementary Figure 2

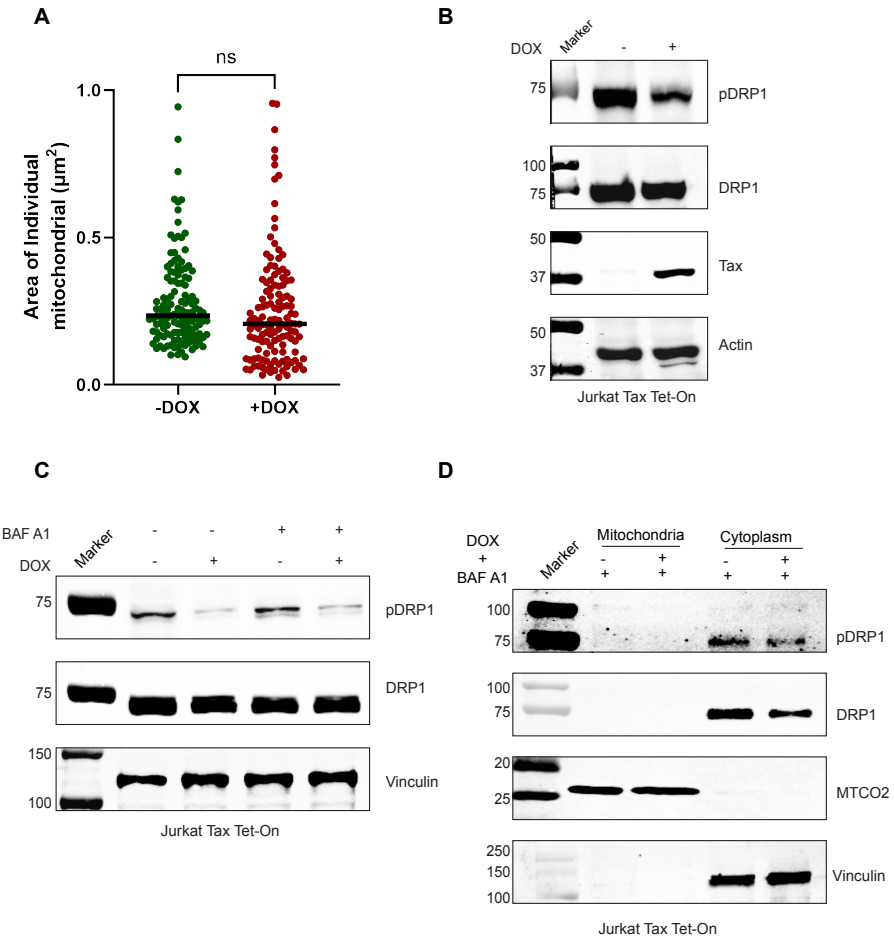

Supplementary Figure 2. DRP1 may not be involved in Tax-induced mitophagy. **(A)** Tax does not change total mitochondrial number as determined by TEM analysis of DOX-treated Jurkat Tax Tet-On cells. Quantification of the area of individual mitochondria in untreated and DOX-treated Jurkat Tax Tet-On cells, where each dot represents a single mitochondria (n=130). The results are expressed as the mean ± SD. Unpaired Student's *t* test with Welch's correction, ns=not significant. **(B)** Immunoblotting was performed with the indicated antibodies using lysates from untreated or DOX-treated (48 h) Jurkat Tax Tet-On cells. **(C)** Immunoblotting was performed with the indicated antibodies using lysates from untreated or DOX and BafA1-treated (48 h) Jurkat Tax Tet-On cells. **(D)** Immunoblotting was performed with the indicated antibodies using mitochondrial and cytoplasmic fractions from untreated or DOX and BafA1-treated (48 h) Jurkat-Tax Tet-on cells.

Supplementary Figure 3

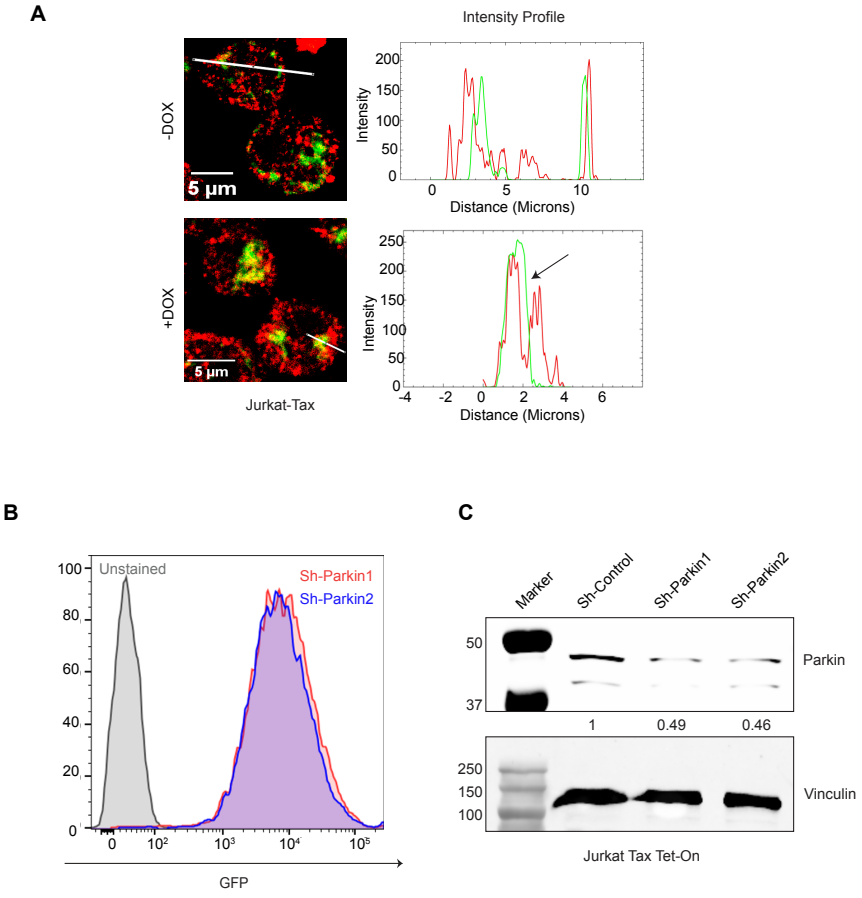

Supplementary Figure 3. Generation of Parkin knockdown Jurkat Tax Tet-On cells. **(A)** Magnified views of Tax and Parkin overlap, highlighting colocalized areas in the zoomed-in sections of untreated and DOX-treated (48 h) Jurkat Tax Tet-On cells. The overlap in intensity profiles (Fiji) indicates Tax and Parkin colocalization. **(B)** Flow cytometry was performed to examine GFP expression in Jurkat Tax Tet-On cells transduced with a lentiviral vector expressing Parkin shRNA**. (C)** Immunoblotting was performed with the indicated antibodies using lysates from Jurkat-Tax Tet-On cells.

Supplementary Figure 4

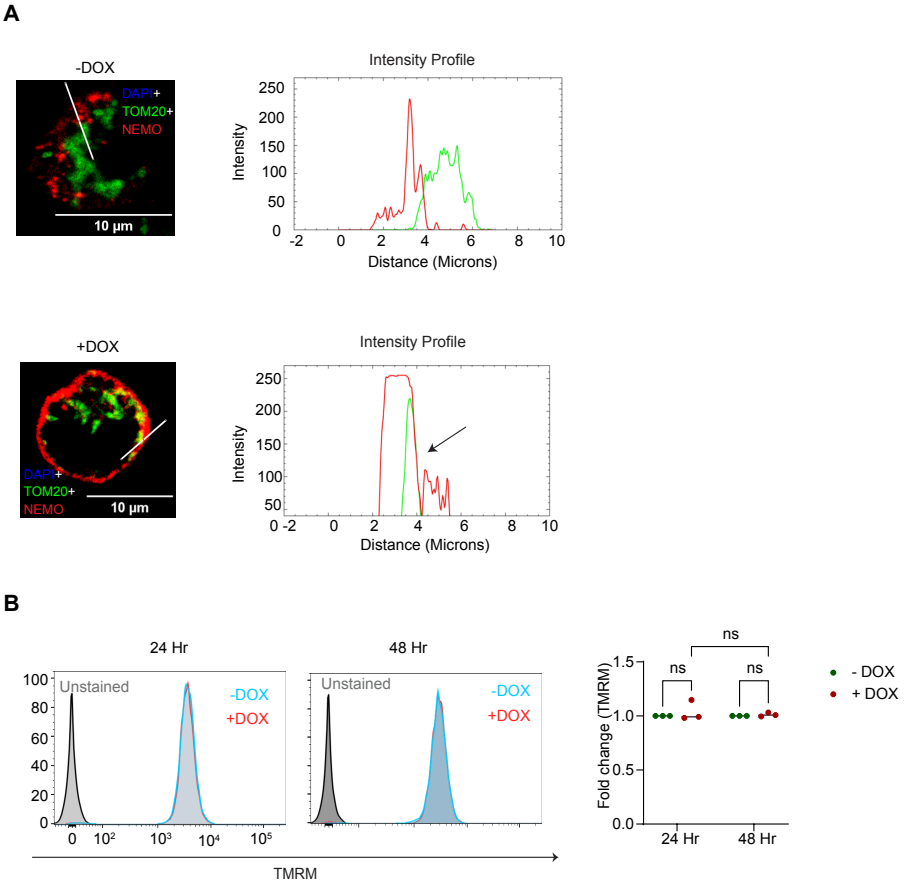

Supplementary Figure 4. Tax promotes NEMO mitochondrial localization. **(A)** Magnified views of NEMO and TOM20 overlap, highlighting colocalized areas in the zoomed-in sections of untreated and DOX-treated (48 h) Jurkat Tax Tet-On cells. The overlap in intensity profiles (Fiji) indicates NEMO and TOM20 colocalization. **(B)** Jurkat Tax M22 Tet-On cells were treated with DOX for the indicated time points and stained with TMRM to assess mitochondrial membrane potential by flow cytometry. Graphical representation indicating the fold change in mitochondrial membrane potential in three biological replicates compared to untreated controls. The results are expressed as the mean ± SD of three independent experiments. ns=not significant. Two-way ANOVA with multiple comparisons test

Supplementary Figure 5

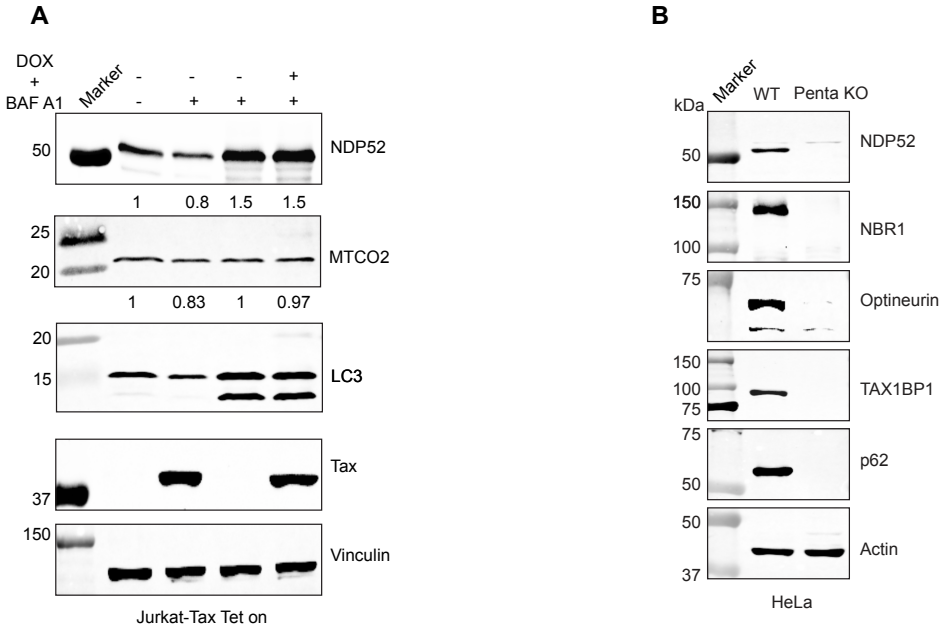

Supplementary Figure 5. Tax triggers the degradation of NDP52 by mitophagy. **(A)** Immunoblotting was performed with the indicated antibodies using lysates from untreated or DOX and BafA1-treated (48 h) Jurkat-Tax Tet-On cells. Protein levels were normalized to the loading control (vinculin) and compared to untreated Jurkat Tax Tet-On cells. **(B)** Immunoblotting was performed with the indicated antibodies using lysates from HeLa WT or pentaKO cells.

Supplementary Figure 6

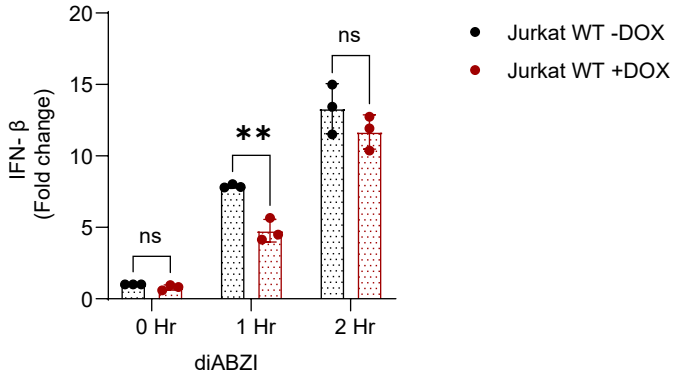

Supplementary Figure 6. DOX treatment does not induce IFN-β in Jurkat cells. qRT-PCR of *Ifnb* mRNA in untreated or DOX-treated Jurkat cells treated with diABZI (1 μM) for the indicated times. The results are expressed as the mean ± SD of three independent experiments. $^{**}P < 0.01$; ns=not significant. Two-way ANOVA with Šídák's multiple comparisons.